splicing in the arsenite-induced motor neuron death assay. The drugs were trichostatin A (a histone deacetyltransferase inhibitor), spliceostatin A (a spliceosomal factor inhibitor) (*26*), and two histone acetyltransferase inhibitors, anacardic acid (*27*) and garcinol (*27*). We identified anacardic acid as protecting against arsenite-induced death of ALS iPSC–derived motor neurons [survival rate, 81.7 ± 4.5% (mean ± SEM) for arsenite-treated ALS motor neurons compared to 97.1 ± 4.8% for arsenite-treated ALS motor neurons pretreated with anacardic acid; $P = 0.048$ by one-way ANOVA] (Fig. 3, G and H).

Anacardic acid decreased TDP-43 mRNA expression in ALS iPSC–derived motor neurons by 147-fold compared to untreated motor neurons ($P = 0.047$ by two-way ANOVA) (Fig. 4A). To investigate the effect of anacardic acid on the production of TDP-43 protein, we treated ALS iPSC–derived motor neuron–containing neural populations with anacardic acid for 48 hours. Anacardic acid reduced the amount of TDP-43 in the insoluble fraction but not in the soluble fraction of ALS iPSC–derived motor neuron–containing neural populations ($P = 8.2 \times 10^{-3}$ by *t* test) (Fig. 4, B and C). Anacardic acid also increased the length of neurites of purified ALS iPSC–derived motor neurons compared to untreated ALS iPSC–derived motor neurons [average neurite length, 75.4 ± 7.5 μm (mean ± SEM) for anacardic acid–treated ALS motor neurons compared to 36.2 ± 2.5 μm for vehicle-treated ALS motor neurons; $P = 0.014$ by two-way ANOVA] (Fig. 4D and fig. S9C). The drug also increased expression of NEFM mRNA (Fig. 4E), down-regulated expression of RNA metabolism–related genes (Fig. 4F), and reversed changes in the tumor necrosis factor–α (TNFα)/nuclear factor κB (NF-κB) signaling pathway (Fig. 4G and fig. S10, A to D).

neuron–containing neural populations differentiated from ALS patient–derived iPSCs. We also observed a punctate cytoplasmic distribution of TDP-43 in ALS iPSC–derived motor neurons and a cellular vulnerability to arsenite treatment, in agreement with the previous report, which showed increased vulnerability of ALS motor neurons to other

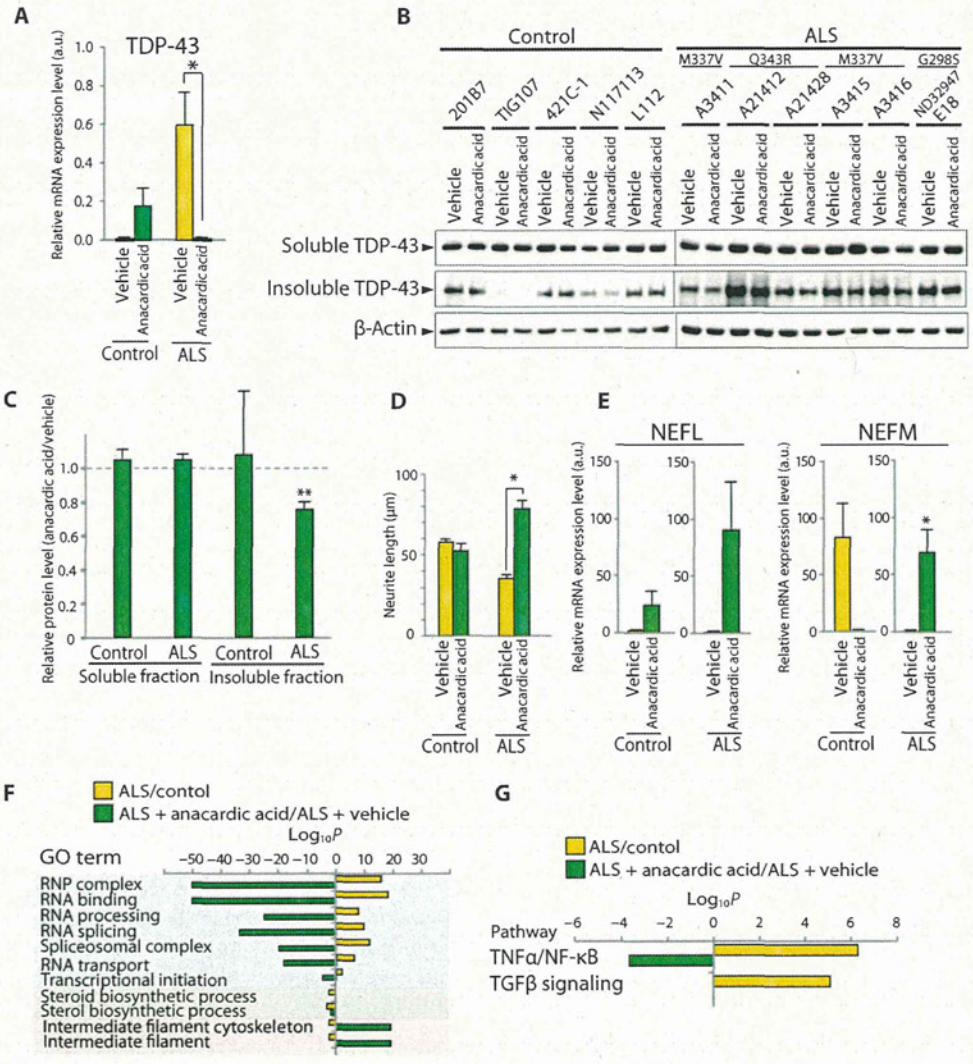

Fig. 4. Anacardic acid–induced phenotypic changes in ALS and control motor neurons. (**A**) qPCR confirmed that 5 μM anacardic acid treatment for 16 hours down-regulated TDP-43 mRNA expression in purified ALS iPSC–derived motor neurons. $P = 0.047$ by two-way ANOVA. Error bars are SEM. (**B**) After treatment with vehicle or 5 μM anacardic acid for 48 hours, cells were lysed, separated into soluble and insoluble fractions, and immunoblotted with TDP-43. (**C**) Quantification of protein band densities after immunoblotting. The dotted line indicates the baseline (vehicle only) of relative protein levels (anacardic acid/vehicle). $P = 8.2 \times 10^{-3}$ by *t* test. Error bars are SEM. (**D**) Neurite length of purified motor neurons was measured 16 hours after treatment with vehicle or 5 μM anacardic acid. $P = 0.014$ by two-way ANOVA. Error bars are SEM. (**E**) qPCR revealed that anacardic acid treatment up-regulated expression of NEFM mRNA in ALS iPSC–derived motor neurons. $P = 0.032$ by *t* test. Error bars are SEM. (**F** and **G**) After purified motor neurons were treated for 16 hours with vehicle or 5 μM anacardic acid, cells were lysed and analyzed by expression array profiling. (Yellow bars) *P* value for significant changes in expression of genes and signaling pathways in ALS versus control iPSC–derived motor neurons was expressed on a logarithmic scale. (Green bars) *P* value for GO terms and signaling pathways of anacardic acid–treated ALS motor neurons compared to vehicle-treated ALS motor neurons was expressed on a logarithmic scale. $^*P < 0.05$, $^{**}P < 0.01$. TGFβ, transforming growth factor–β.

DISCUSSION

We found cellular and molecular phenotypes associated with ALS in motor neurons derived from ALS patient–specific iPSCs harboring mutant TDP-43. Consistent with a previous study describing the generation of iPSCs from ALS patients carrying the TDP-43 M337V mutation (*13*), in our study, the TDP-43 mutation did not affect the differentiation of ALS iPSCs into motor neurons. We report an increase in insoluble TDP-43 in motor

cellular stressors (*13*). There were, however, two differences between these studies. In the previous study (*13*), TDP-43 mRNA expression was similar between control iPSC–derived motor neuron culture and iPSC-derived motor neuron culture from ALS patients with the TDP-43 (M337V) mutation. In contrast, we found that TDP-43 mRNA was up-regulated in ALS iPSC–derived motor neurons with the same TDP-43 M337V mutation or with two other mutations (Q343R and G298S) compared to control iPSC–derived motor neurons. We speculate that there may be several reasons for this difference between the two studies. First, we analyzed multiple iPSC lines to account for clonal variation. We found that in one ALS iPSC line with the TDP-43 M337V mutation, TDP-43 mRNA expression was close to control, whereas the other ALS iPSC lines containing the same mutation showed up-regulation of TDP-43 mRNA. Second, we analyzed the expression of TDP-43 mRNA in purified ALS iPSC–derived motor neurons to avoid contamination with other cell types. Another difference between the two studies was the result of the lactate dehydrogenase cytotoxicity assay (fig. S11). Unlike the previous study, we found no difference in survival between control and ALS motor neurons using this assay. We speculate that this discrepancy stemmed from the fact that we used multiple iPSC lines from three different ALS patients and that this reduced the impact of clonal variation. Further progress in culture methods for motor neurons might make it possible to recapitulate ALS motor neuron death under basal conditions.

In our study, we used multiple iPSC lines from three different ALS patients for our phenotyping assays to address the challenge of clonal variation because we discovered variations even between iPSC lines derived from the same ALS patient. Although we did not use all of the iPSC clones from all ALS patients in all of the assays, we used at least two clones from each ALS patient in each phenotyping assay including immunoblot analysis of insoluble TDP-43, neurite length quantification, and quantitative polymerase chain reaction (qPCR) analysis of TDP-43 mRNA. In the drug screening assay, we used selected ALS iPSC lines and tested a positive hit on phenotyped clones that were not included in the primary screening assay. We demonstrated that the results of drug screening were not specific to the subset of screened clones. Clonal variation of iPSC lines continues to be an obstacle for cellular modeling of disease.

We found that mutant TDP-43 was more insoluble and more prone to forming aggregates than wild-type TDP-43. These properties may contribute to loss of the negative feedback loop that autoregulates synthesis of TDP-43 (*8*), which could in turn lead to increased expression of TDP-43 mRNA and protein. Increased amounts of TDP-43 protein bound to other RNA binding proteins such as the spliceosomal factor SNRPB2 could lead to perturbation of RNA metabolism. We generated iPSCs from three ALS patients carrying distinct TDP-43 mutations: Q343R, M337V, and G298S. These mutations and other mutations are located in the glycine-rich domain of TDP-43 (*28*). We speculate that mutations in the glycine-rich domain of TDP-43 may disrupt the interaction of mutant TDP-43 with other proteins or RNAs, leading to up-regulation of TDP-43 mRNA, an increase in mutant TDP-43 protein, and the formation of more aggregates. In our study, mutant TDP-43 was more sensitive to oxidative stress, which increased the amount of insoluble TDP-43 and hence aggregate formation. Anacardic acid may reverse ALS-associated phenotypes potentially by down-regulation of TDP-43 mRNA expression. However, anacardic acid might partially exert its effect through the suppression of other genes that are regulated by NF-κB (*29*) or through control of redox signaling (*30*) because pathogenic TDP-43 has been implicated in both pathways (*23*, *25*).

In summary, we identified cellular and molecular phenotypes associated with ALS using ALS patient–specific iPSC–derived motor neurons and set up a screening assay that identified anacardic acid as a drug that could reverse some of the ALS phenotypes. Our data suggest that ALS iPSC–derived motor neurons may be useful for elucidating disease pathogenesis and for identifying new candidate drugs.

MATERIALS AND METHODS

Derivation of patient-specific fibroblasts

Control and ALS-derived human dermal fibroblasts (HDFs) other than ND32947 were generated from explants of 3-mm dermal biopsies. ND32947 was obtained from Coriell Institute (Camden, NJ). After 1 to 2 weeks, fibroblast outgrowths from the explants were passaged.

iPSC generation

Human complementary DNAs for reprogramming factors were transduced in HDF with retrovirus (Sox2, Klf4, Oct3/4, and/or c-Myc) or episomal vectors (Sox2, Klf4, Oct3/4, L-Myc, Lin28, short hairpin RNA for p53). Several days after transduction, fibroblasts were harvested and replated on an SNL feeder layer. On the next day, the medium was changed to primate embryonic stem cell medium (ReproCELL) supplemented with basic fibroblast growth factor (4 ng/ml) (Wako Chemicals). The medium was changed every other day. Thirty days after transduction, iPSC colonies were picked up.

Immunocytochemistry

Cells were fixed in 4% paraformaldehyde (pH 7.4) for 30 min at room temperature and rinsed with phosphate-buffered saline (PBS). The cells were permeabilized in PBS containing 0.2% Triton X-100 for 10 min at room temperature, followed by rinsing with PBS. Nonspecific binding was blocked with PBS containing 10% donkey serum for 60 min at room temperature. Cells were incubated with primary antibodies overnight at 4°C and then labeled with appropriate fluorescently tagged secondary antibodies. DAPI (4′,6-diamidino-2-phenylindole) (Life Technologies) was used to label nuclei. Fluorescence images were acquired on DeltaVision (Applied Precision). The following primary antibodies were used in this assay: Nanog (R&D Systems, 1:10), SSEA-4 (Millipore, 1:100), SOX-17 (R&D Systems, 1:50), αSMA (DAKO A/S, 1:500), Tuj1 (Covance, 1:2000), Islet-1 (Developmental Studies Hybridoma Bank, 1:50), HB9 (Epitomics, 1:2000), ChAT (Millipore, 1:100), SMI-32 (Covance, 1:500), synapsin (Millipore, 1:500), MAP2 (Millipore, 1:200), GFAP (DAKO, 1:1000), TDP-43 (Proteintech, 1:500), and SNRPB2 (Proteintech, 1:300).

Quantitating the number of TDP-43 aggregates in cytoplasm

Differentiated motor neurons were visualized with anti–SMI-32 antibody. Nuclei were then stained with DAPI. The number of TDP-43 dots in cytoplasm was quantified by IN Cell Analyzer 6000 (GE Healthcare). The TDP-43 dot was defined by a size of more than 0.324 μm.

Immunoprecipitation

After being washed with PBS, cells cultured in 24-well plates were solubilized for 30 min on ice in immunoprecipitation assay buffer

(50 mM tris-HCl, 150 mM NaCl, 1 mM EDTA, 1% Triton X-100, 0.1% SDS, and 0.1% sodium deoxycholate) with a protease inhibitor cocktail and a phosphatase inhibitor with Bioruptor (high mode, ON: 30 s, OFF: 60 s, 20 times). Insoluble fraction was collected by centrifugation (15,000 rpm, 3 min), in which the supernatant was defined as soluble fraction, and lysed in SDS lysis solution (50 mM tris-HCl, 10 mM EDTA, 1% SDS) with Bioruptor. Soluble lysates were incubated overnight with protein G–Sepharose bound to anti–TDP-43 antibody (Abnova). Lysates from insoluble fraction were diluted to 10% by dilution buffer (50 mM tris-HCl, 167 mM NaCl, 1.1% Triton X-100, and 0.11% sodium deoxycholate) including phosphatase inhibitor and then incubated overnight by protein G–Sepharose bound to anti–TDP-43 antibody (Abnova). Sepharose beads were collected by brief centrifugation and washed with TBS buffer (50 mM tris-HCl, 150 mM NaCl, pH 7.4) three times. Immunoprecipitated material was eluted by boiling for 3 min in 2× sample buffer [125 mM tris-HCl (pH 6.8), 4% SDS, 20% glycerol, 0.004% bromophenol blue].

Induction of motor neurons by quick embryoid body–like aggregate method (SFEBq)

Human iPSCs were dissociated to single cells and quickly reaggregated in low cell adhesion U-shaped 96-well plates (Lipidure-Coat Plate A-U96, NOF Corporation). Aggregations were cultured in 5% DFK medium [5% KSR Medium (DFK5%), Dulbecco's modified Eagle's medium/Ham's F12 (Sigma-Aldrich), 5% KSR (Invitrogen), minimum essential medium–nonessential amino acids (Invitrogen), L-glutamine (Sigma-Aldrich), 2-mercaptoethanol (Wako)] with 2 μM dorsomorphin and SB431542 in a neural inductive stage (P1) for 12 days. After patterning with neurobasal medium supplemented with B27, 1 μM retinoic acid, Sonic Hedgehog (100 to 500 ng/ml), and fibroblast growth factor 2 (12.5 ng/ml), the aggregates were adhered to Matrigel (BD Biosciences)–coated dishes on day 22. Adhesive embryoid bodies were cultured in neurobasal medium with brain-derived neurotrophic factor (10 ng/ml), glial cell line–derived neurotrophic factor (10 ng/ml), and NT-3 (10 ng/ml) in P2 culture. They were separated from the dish by Accutase, dissociated into a small clump or single cells, and cultured at 500,000 cells per well on Matrigel-coated 24-well dishes on day 35 as P3 maturation stage.

SUPPLEMENTARY MATERIALS

www.sciencetranslationalmedicine.org/cgi/content/full/4/145/145ra104/DC1
Materials and Methods
Fig. S1. ESC marker, genotype, and karyotype analysis.
Fig. S2. Transgene expression.
Fig. S3. In vitro three-germ layer and teratoma assay.
Fig. S4. Bisulfite genomic sequencing of the promoter regions of Nanog and Oct4.
Fig. S5. Comparison of global gene expression profiles of human iPSCs.
Fig. S6. Motor neuron differentiation and functional assay of motor neurons.
Fig. S7. Estimation of neuronal differentiation from control and ALS iPSCs.
Fig. S8. Motor neuron purification for gene expression analysis.
Fig. S9. Decreased neurite length of ALS motor neurons.
Fig. S10. Signaling pathways significantly activated in ALS motor neurons.
Fig. S11. Cell viability and cytotoxicity.
Table S1. List of clones for human iPSC lines.
Table S2. Correlation coefficients of global gene expression in human iPSC lines.
Table S3. GO analysis of microarray data (fold change >1.2) ALS UP.
Table S4. GO analysis of microarray data (fold change >1.2) ALS DOWN.
Table S5. Genes identified as significantly increased ($P < 0.05$) with >1.2-fold change in motor neurons derived from ALS human iPSCs.
Table S6. Genes identified as significantly decreased ($P < 0.05$) with >1.2-fold change in motor neurons derived from ALS human iPSCs.
Table S7. Primers list.
References

REFERENCES AND NOTES

1. L. I. Bruijn, T. M. Miller, D. W. Cleveland, Unraveling the mechanisms involved in motor neuron degeneration in ALS. *Annu. Rev. Neurosci.* **27**, 723–749 (2004).
2. J. D. Rothstein, Current hypotheses for the underlying biology of amyotrophic lateral sclerosis. *Ann. Neurol.* **65** (Suppl. 1), S3–S9 (2009).
3. M. Neumann, D. M. Sampathu, L. K. Kwong, A. C. Truax, M. C. Micsenyi, T. T. Chou, J. Bruce, T. Schuck, M. Grossman, C. M. Clark, L. F. McCluskey, B. L. Miller, E. Masliah, I. R. Mackenzie, H. Feldman, W. Feiden, H. A. Kretzschmar, J. Q. Trojanowski, V. M. Lee, Ubiquitinated TDP-43 in frontotemporal lobar degeneration and amyotrophic lateral sclerosis. *Science* **314**, 130–133 (2006).
4. T. Arai, M. Hasegawa, H. Akiyama, K. Ikeda, T. Nonaka, H. Mori, D. Mann, K. Tsuchiya, M. Yoshida, Y. Hashizume, T. Oda, TDP-43 is a component of ubiquitin-positive tau-negative inclusions in frontotemporal lobar degeneration and amyotrophic lateral sclerosis. *Biochem. Biophys. Res. Commun.* **351**, 602–611 (2006).
5. I. R. Mackenzie, E. H. Bigio, P. G. Ince, F. Geser, M. Neumann, N. J. Cairns, L. K. Kwong, M. S. Forman, J. Ravits, H. Stewart, A. Eisen, L. McClusky, H. A. Kretzschmar, C. M. Monoranu, J. R. Highley, J. Kirby, T. Siddique, P. J. Shaw, V. M. Lee, J. Q. Trojanowski, Pathological TDP-43 distinguishes sporadic amyotrophic lateral sclerosis from amyotrophic lateral sclerosis with *SOD1* mutations. *Ann. Neurol.* **61**, 427–434 (2007).
6. E. Kabashi, L. Lin, M. L. Tradewell, P. A. Dion, V. Bercier, P. Bourgouin, D. Rochefort, S. Bel Hadj, H. D. Durham, C. Vande Velde, G. A. Rouleau, P. Drapeau, Gain and loss of function of ALS-related mutations of *TARDBP* (TDP-43) cause motor deficits in vivo. *Hum. Mol. Genet.* **19**, 671–683 (2010).
7. M. J. Strong, The evidence for altered RNA metabolism in amyotrophic lateral sclerosis (ALS). *J. Neurol. Sci.* **288**, 1–12 (2010).
8. Y. M. Ayala, L. De Conti, S. E. Avendaño-Vázquez, A. Dhir, M. Romano, A. D'Ambrogio, J. Tollervey, J. Ule, M. Baralle, E. Buratti, F. E. Baralle, TDP-43 regulates its mRNA levels through a negative feedback loop. *EMBO J.* **30**, 277–288 (2011).
9. L. Liu-Yesucevitz, A. Bilgutay, Y. J. Zhang, T. Vanderweyde, A. Citro, T. Mehta, N. Zaarur, A. McKee, R. Bowser, M. Sherman, L. Petrucelli, B. Wolozin, Tar DNA binding protein-43 (TDP-43) associates with stress granules: Analysis of cultured cells and pathological brain tissue. *PLoS One* **5**, e13250 (2010).
10. N. J. Rutherford, Y. J. Zhang, M. Baker, J. M. Gass, N. A. Finch, Y. F. Xu, H. Stewart, B. J. Kelley, K. Kuntz, R. J. Crook, J. Sreedharan, C. Vance, E. Sorenson, C. Lippa, E. H. Bigio, D. H. Geschwind, D. S. Knopman, H. Mitsumoto, R. C. Petersen, N. R. Cashman, M. Hutton, C. E. Shaw, K. B. Boylan, B. Boeve, N. R. Graff-Radford, Z. K. Wszolek, R. J. Caselli, D. W. Dickson, I. R. Mackenzie, L. Petrucelli, R. Rademakers, Novel mutations in *TARDBP* (TDP-43) in patients with familial amyotrophic lateral sclerosis. *PLoS Genet.* **4**, e1000193 (2008).
11. H. Inoue, S. Yamanaka, The use of induced pluripotent stem cells in drug development. *Clin. Pharmacol. Ther.* **89**, 655–661 (2011).
12. J. T. Dimos, K. T. Rodolfa, K. K. Niakan, L. M. Weisenthal, H. Mitsumoto, W. Chung, G. F. Croft, G. Saphier, R. Leibel, R. Goland, H. Wichterle, C. E. Henderson, K. Eggan, Induced pluripotent stem cells generated from patients with ALS can be differentiated into motor neurons. *Science* **321**, 1218–1221 (2008).
13. B. Bilican, A. Serio, S. J. Barmada, A. L. Nishimura, G. J. Sullivan, M. Carrasco, H. P. Phatnani, C. A. Puddifoot, D. Story, J. Fletcher, I. H. Park, B. A. Friedman, G. Q. Daley, D. J. Wyllie, G. E. Hardingham, I. Wilmut, S. Finkbeiner, T. Maniatis, C. E. Shaw, S. Chandran, Mutant induced pluripotent stem cell lines recapitulate aspects of TDP-43 proteinopathies and reveal cell-specific vulnerability. *Proc. Natl. Acad. Sci. U.S.A.* **109**, 5803–5808 (2012).
14. K. Takahashi, K. Tanabe, M. Ohnuki, M. Narita, T. Ichisaka, K. Tomoda, S. Yamanaka, Induction of pluripotent stem cells from adult human fibroblasts by defined factors. *Cell* **131**, 861–872 (2007).
15. K. Okita, Y. Matsumura, Y. Sato, A. Okada, A. Morizane, S. Okamoto, H. Hong, M. Nakagawa, K. Tanabe, K. Tezuka, T. Shibata, T. Kunisada, M. Takahashi, J. Takahashi, H. Saji, S. Yamanaka, A more efficient method to generate integration-free human iPS cells. *Nat. Methods* **8**, 409–412 (2011).
16. T. Wada, M. Honda, I. Minami, N. Tooi, Y. Amagai, N. Nakatsuji, K. Aiba, Highly efficient differentiation and enrichment of spinal motor neurons derived from human and monkey embryonic stem cells. *PLoS One* **4**, e6722 (2009).
17. M. C. Marchetto, A. R. Muotri, Y. Mu, A. M. Smith, G. G. Cezar, F. H. Gage, Non-cell-autonomous effect of human $SOD1^{G37R}$ astrocytes on motor neurons derived from human embryonic stem cells. *Cell Stem Cell* **3**, 649–657 (2008).
18. C. Bergeron, K. Beric-Maskarel, S. Muntasser, L. Weyer, M. J. Somerville, M. E. Percy, Neurofilament light and polyadenylated mRNA levels are decreased in amyotrophic lateral sclerosis motor neurons. *J. Neuropathol. Exp. Neurol.* **53**, 221–230 (1994).

19. K. Watanabe, D. Kamiya, A. Nishiyama, T. Katayama, S. Nozaki, H. Kawasaki, Y. Watanabe, K. Mizuseki, Y. Sasai, Directed differentiation of telencephalic precursors from embryonic stem cells. *Nat. Neurosci.* **8**, 288–296 (2005).
20. E. B. Lee, V. M. Lee, J. Q. Trojanowski, Gains or losses: Molecular mechanisms of TDP43-mediated neurodegeneration. *Nat. Rev. Neurosci.* **13**, 38–50 (2012).
21. J. R. Tollervey, T. Curk, B. Rogelj, M. Briese, M. Cereda, M. Kayikci, J. König, T. Hortobágyi, A. L. Nishimura, V. Zupunski, R. Patani, S. Chandran, G. Rot, B. Zupan, C. E. Shaw, J. Ule, Characterizing the RNA targets and position-dependent splicing regulation by TDP-43. *Nat. Neurosci.* **14**, 452–458 (2011).
22. M. Polymenidou, C. Lagier-Tourenne, K. R. Hutt, S. C. Huelga, J. Moran, T. Y. Liang, S. C. Ling, E. Sun, E. Wancewicz, C. Mazur, H. Kordasiewicz, Y. Sedaghat, J. P. Donohue, L. Shiue, C. F. Bennett, G. W. Yeo, D. W. Cleveland, Long pre-mRNA depletion and RNA missplicing contribute to neuronal vulnerability from loss of TDP-43. *Nat. Neurosci.* **14**, 459–468 (2011).
23. V. Swarup, D. Phaneuf, N. Dupré, S. Petri, M. Strong, J. Kriz, J. P. Julien, Deregulation of TDP-43 in amyotrophic lateral sclerosis triggers nuclear factor κB–mediated pathogenic pathways. *J. Exp. Med.* **208**, 2429–2447 (2011).
24. W. Guo, Y. Chen, X. Zhou, A. Kar, P. Ray, X. Chen, E. J. Rao, M. Yang, H. Ye, L. Zhu, J. Liu, M. Xu, Y. Yang, C. Wang, D. Zhang, E. H. Bigio, M. Mesulam, Y. Shen, Q. Xu, K. Fushimi, J. Y. Wu, An ALS-associated mutation affecting TDP-43 enhances protein aggregation, fibril formation and neurotoxicity. *Nat. Struct. Mol. Biol.* **18**, 822–830 (2011).
25. T. J. Cohen, A. W. Hwang, T. Unger, J. Q. Trojanowski, V. M. Lee, Redox signalling directly regulates TDP-43 via cysteine oxidation and disulphide cross-linking. *EMBO J.* **31**, 1241–1252 (2011).
26. D. Kaida, H. Motoyoshi, E. Tashiro, T. Nojima, M. Hagiwara, K. Ishigami, H. Watanabe, T. Kitahara, T. Yoshida, H. Nakajima, T. Tani, S. Horinouchi, M. Yoshida, Spliceostatin A targets SF3b and inhibits both splicing and nuclear retention of pre-mRNA. *Nat. Chem. Biol.* **3**, 576–583 (2007).
27. F. J. Dekker, H. J. Haisma, Histone acetyl transferases as emerging drug targets. *Drug Discov. Today* **14**, 942–948 (2009).
28. G. S. Pesiridis, V. M. Lee, J. Q. Trojanowski, Mutations in TDP-43 link glycine-rich domain functions to amyotrophic lateral sclerosis. *Hum. Mol. Genet.* **18**, R156–R162 (2009).
29. B. Sung, M. K. Pandey, K. S. Ahn, T. Yi, M. M. Chaturvedi, M. Liu, B. B. Aggarwal, Anacardic acid (6-nonadecyl salicylic acid), an inhibitor of histone acetyltransferase, suppresses expression of nuclear factor-κB–regulated gene products involved in cell survival, proliferation, invasion, and inflammation through inhibition of the inhibitory subunit of nuclear factor-κBα kinase, leading to potentiation of apoptosis. *Blood* **111**, 4880–4891 (2008).
30. M. Toyomizu, K. Okamoto, T. Ishibashi, Z. Chen, T. Nakatsu, Uncoupling effect of anacardic acids from cashew nut shell oil on oxidative phosphorylation of rat liver mitochondria. *Life Sci.* **66**, 229–234 (2000).

Acknowledgments: We thank our co-workers and collaborators; S. L. Pfaff for providing plasmids; M. Kawada, Y. Karatsu, and T. Enami for technical assistance; and K. Murai for editing the manuscript. **Funding:** This research was funded in part by a grant from the Funding Program for World-Leading Innovative R&D on Science and Technology (FIRST Program) of the Japan Society for the Promotion of Science (S. Yamanaka), a grant from the JST Yamanaka iPS cell special project (S. Yamanaka and H. Inoue), Core Research for Evolutional Science and Technology (H. Inoue), Grant-in-Aid from the Ministry of Health and Labour (R.T. and H. Inoue), a Grant-in-Aid for Scientific Research on Innovative Area "Foundation of Synapse and Neurocircuit Pathology" (22110007) from the Ministry of Education, Culture, Sports, Science and Technology of Japan (H. Inoue), and a research grant from the Novartis Foundation for Gerontological Research (H. Inoue). **Author contributions:** H. Inoue planned the project; H. Inoue, N.E., and S.K. designed the experiments; S. Yamanaka, H. Inoue, N.E., and S.K. wrote the manuscript; K.Y., S. Yamawaki, M.N., S.S., K.M., K. Okamoto, H.T., A.T., K.H., and R.T. recruited patients; N.E., S.K., K. Takahashi, K.M., F.A., K.Y., T. Kondo, K. Tsukita, K. Okita, I.A., H. Inoue, and S. Yamanaka generated and characterized iPSCs; T. Aoi conducted karyotyping; A.W. performed methylation analysis of iPSCs; Y.Y. performed immunohistochemical analysis of teratomas; N.E., S.K., K. Takahashi, K.M., and F.A. performed generation and characterization of human motor neurons; A.M. and J.T. provided technical support for neuronal differentiation; D.W. performed whole-cell patch clamp; H.H. and T. Kaneko generated lentivirus vectors with high titers; T.Y. supported the microarray analysis; H. Ito and T. Ayaki performed immunohistochemistry of human spinal cords; M.Y. provided spliceostatin A; A.K. provided human materials; T. Nakahata provided NOG mice; T. Nonaka and M.H. provided antibodies, plasmids, and scientific discussions; R.T. provided scientific discussions; M.C.N.M. and F.H.G. provided plasmids and scientific discussions. **Competing interests:** A.T. is a paid consultant to Chugai Pharmaceutical Co. Ltd. S. Yamanaka is a member of the scientific advisory boards of iPierian, iPS Academia Japan, and Megakaryon Corporation. H. Inoue, N.E., S.K., and K. Tsukita have filed a patent (Prophylactic and therapeutic drug for amyotrophic lateral sclerosis and method of screening, 61/587,323) related to this work. The other authors declare that they have no competing interests.

Submitted 23 March 2012
Accepted 13 July 2012
Published 1 August 2012
10.1126/scitranslmed.3004052

Citation: N. Egawa, S. Kitaoka, K. Tsukita, M. Naitoh, K. Takahashi, T. Yamamoto, F. Adachi, T. Kondo, K. Okita, I. Asaka, T. Aoi, A. Watanabe, Y. Yamada, A. Morizane, J. Takahashi, T. Ayaki, H. Ito, K. Yoshikawa, S. Yamawaki, S. Suzuki, D. Watanabe, H. Hioki, T. Kaneko, K. Makioka, K. Okamoto, H. Takuma, A. Tamaoka, K. Hasegawa, T. Nonaka, M. Hasegawa, A. Kawata, M. Yoshida, T. Nakahata, R. Takahashi, M. C. N. Marchetto, F. H. Gage, S. Yamanaka, H. Inoue, Drug screening for ALS using patient-specific induced pluripotent stem cells. *Sci. Transl. Med.* **4**, 145ra104 (2012).

J Neuropathol Exp Neurol

Vol. 71, No. 7
July 2012
pp. 625–630

ORIGINAL ARTICLE

α-Synuclein Pathology in the Amyotrophic Lateral Sclerosis/Parkinsonism Dementia Complex in the Kii Peninsula, Japan

Yasumasa Kokubo, MD, PhD, Akira Taniguchi, MD, Masato Hasegawa, PhD, Yuma Hayakawa, Satoru Morimoto, MD, Misao Yoneda, PhD, Yoshihumi Hirokawa, MD, PhD, Taizo Shiraishi, MD, PhD, Yuko Saito, MD, PhD, Shigeo Murayama, MD, PhD, and Shigeki Kuzuhara, MD, PhD

Abstract

α-Synuclein pathology was examined in the brains and spinal cords of 10 patients with amyotrophic lateral sclerosis (ALS)/parkinsonism-dementia complex (PDC) in the Kii Peninsula, Japan. Various types of phosphorylated α-synuclein–positive structures including neuronal cytoplasmic inclusions, dystrophic neurites, and glial cytoplasmic inclusions were found in all ALS/PDC cases. There were phosphorylated α-synuclein–positive neurons in 8 cases (80%), and the amygdala was most severely affected. Phosphorylated α-synuclein was distributed mainly in the limbic system and brainstem; tau pathology was more prevalent than α-synuclein pathology in most affected areas. In the substantia nigra, periaqueductal gray, locus coeruleus, raphe nuclei, dorsal nucleus of the vagus nerve, hypoglossal nucleus or ventral horn, and intermediolateral nucleus of the spinal cord, α-synuclein pathology was more predominant than tau pathology in only 1 or 2 patients. Phosphorylated α-synuclein– positive structures were not found in the molecular layer of the cerebellum. Phosphorylated α-synuclein frequently colocalized with tau in neuron cell bodies, neurites, and glia. Immunoblots of sarkosyl-insoluble fractions extracted from the brain of 1 patient showed a triplet of α-synuclein–immunoreactive bands that were ubiquitinated. These results suggest that interaction between tau and α-synuclein be involved in the pathogenesis of Kii ALS/PDC.

Key Words: α-Synuclein, Amyotrophic lateral sclerosis, Guam, Kii Peninsula, Parkinsonism-dementia complex, Tau.

From the Departments of Neurology (YK, AT), and Pathology (MY, YHi, TS), Mie University Graduate School of Medicine, Mie; Department of Molecular Neurobiology (MH), Tokyo Metropolitan Institute of Medical Science; Department of Neuropathology (SMo, SMu), Metropolitan Institute of Gerontology; Department of Neuropathology (YS), National Center of Neurology and Psychiatry, Tokyo; and Department of Medical Welfare (SK), Suzuka University of Medical Science, Mie, Japan.

Send correspondence and reprint requests to: Yasumasa Kokubo, MD, PhD, Department of Neurology, Mie University Graduate School of Medicine, 2-174 Edobashi, Tsu, Mie 514-8507, Japan; E-mail: kokubo-y@clin.medic.mie-u.ac.jp

Yuma Hayakawa is a medical student at the Mie University School of Medicine, Mie, Japan.

This study was supported in part by a Grant-in-Aid of the Nagao Memorial Fund, the Mie Medical Fund, by a Grant-in-Aid of the Research Committee of CNS Degenerative Diseases and Muro Disease (Kii ALS/PDC), the Ministry of Health, Labor and Welfare, Japan (Grant 21210301 to Y.K.), and by a Grant-in-Aid for Scientific Research from the Ministry of Education, Science, Sports and Culture, Japan.

INTRODUCTION

Amyotrophic lateral sclerosis/parkinsonism-dementia complex (ALS/PDC) is a neurodegenerative disease endemic to Guam and the Kii Peninsula of Japan (1–3). The clinical picture of ALS/PDC is a unique combination of parkinsonism, dementia, and symptoms of upper and lower motor neuronal dysfunction. Neuropathologic findings of ALS/PDC include numerous neurofibrillary tangles (NFTs) associated with nerve cell loss in the cerebral cortex and brainstem in addition to ALS pathology. Our investigation of the topographical distribution of NFTs suggested that ALS and PDC in the Kii Peninsula comprise part of a spectrum of tauopathies (4).

α-Synuclein is a presynaptic protein. Phosphorylated α-synuclein is the main component of Lewy bodies (LBs) that are characteristic of Parkinson disease and dementia with LBs (DLB), and of the glial cytoplasmic inclusions found in multiple system atrophy (5, 6). In Guamanian patients with PDC, α-synuclein–positive structures have been detected in the amygdala in approximately 40% of cases (7, 8) and in the cerebellum in more than 60% of cases (9). In this report, we examined phosphorylated α-synuclein immunoreactivity in the brains and spinal cords from 10 patients with ALS/PDC from the Kii Peninsula (Kii ALS/PDC) and analyzed biochemical aspects of α-synuclein from 1 patient.

MATERIALS AND METHODS

Cases

We examined 10 patients with neuropathologically verified Kii ALS/PDC (mean age, 69.1 years; range, 60–77 years). Demographic features and clinical manifestations are listed in Table 1. This study was approved by the ethics committee of Mie University Graduate School of Medicine. Informed consent was obtained from the patients or their families.

Neuropathology and Immunohistochemistry

The brains and spinal cords were fixed in formalin solution for 2 to 3 weeks. The brains were sliced into coronal sections and the spinal cords were sliced axially. Paraffin-embedded samples were cut into 9-μm-thick sections for hematoxylin and eosin, Klüver-Barrera, and Gallyas-Braak staining. All histologic samples showed numerous NFTs

TABLE 1. Clinical Data

Case No.	Age, y	Sex	Duration of Illness, y	Phenotype		
				A	P	D
1	70	F	13	+	−	−
2	63	F	5	+	−	−
3	66	F	3	+	−	−
4	65	M	3	+	−	+
5	77	M	7	+	−	+
6	70	F	8	+	+	+
7	60	F	7	+	+	+
8	76	F	6	+	+	+
9	70	F	14	−	+	+
10	74	M	6	−	+	+

A, Amyotrophic lateral sclerosis; P, parkinsonism, D, dementia; F, female; M, male; −, absent; +, present.

without senile plaques. Nerve cell loss was chiefly in the temporal cortex, frontal cortex, and the nuclei of the brainstem. Loss of anterior horn cells and degeneration of pyramidal tracts were common features.

Six-micrometer-thick sections were prepared for immunohistochemical studies. Immunostaining was performed using the avidin-biotin-peroxidase complex (ABC) method with a Vectastain ABC kit (Vector Laboratories, Burlingame, CA). The antibodies used and their dilutions were as follows: anti-phosphorylated α-synuclein antibody specifically recognizes phosphorylation at Ser-129 (PSer129, 1:5000; monoclonal; Wako, Osaka, Japan) and anti–phosphorylated tau antibody (AT8, 1:100; monoclonal, Innogenetics, Ghent, Belgium). Regions selected for evaluation are shown in Table 2. To evaluate the phosphorylated α-synuclein–positive structures and phosphorylated tau-positive structures, scores ranging from (−) to (+++) were assigned according to the number of structures in the area of maximum density. Phosphorylated α-synuclein–positive and phosphorylated tau-positive neurons were counted in 100× microscopic fields. Densities of phosphorylated α-synuclein–positive were scored as follows: −, 0; ±, 1; +, 2 to 5; ++, 6 to 10; +++, more than 10/field. Densities of phosphorylated tau-positive neurons were scored as follows: −, 0; +, 1 to 10; ++, 11 to 20; +++, more than 20/field. Colocalization of phosphorylated α-synuclein and phosphorylated tau was determined in sections double-labeled with PSer129 antibody and AT8 antibody using immunofluorescent substrate (Alexa Fluor 488 and 546; Life Technologies, Carlsbad, CA).

Western Blot

Sarkosyl-insoluble α-synuclein was extracted from the hippocampus of case 10. Sarkosyl-insoluble α-synuclein was prepared as previously described (10, 11) with slight modifications. Briefly, frozen brain tissue samples were homogenized in a 20-fold volume of buffer A (10 mmol/L Tris, pH 7.5, 1 mmol/L EGTA, 1 mmol/L dithiothreitol, 10% sucrose) containing 1% Triton X-100, incubated for 30 minutes at 37°C and spun at 100,000 × *g* for 30 minutes at 25°C. The resultant pellets were subsequently homogenized in buffer A containing 1% sarkosyl, incubated at 37°C for 30 minutes, and centrifuged 100,000 × *g* for 30 minutes. The sarkosyl-insoluble pellet was homogenized in 4 volumes of buffer A containing 1% CHAPS and spun at 100,000 × *g* for 20 minutes. The pellet was sonicated in 1 volume of 8 mol/L urea and spun at 100,000 × *g* for 20 minutes. The supernatant was mixed with an equal volume of 2× SDS sample buffer and treated at 100°C for 3 minutes. Aliquots of the samples were separated on a 10% or 15% sodium dodecyl sulfate (SDS)–polyacrylamide gel and transferred to a polyvinylidene difluoride membrane. The membrane was then probed with PSer129 (1:2000) and phosphorylation-independent anti–α-synuclein antibody (Syn 102: mouse monoclonal antibody, epitope location on α-synuclein residues 131–140) (12).

In vitro ubiquitination of α-synuclein was performed as previously described (12) with minor modifications. Briefly, 20 μg of human recombinant α-synuclein and 2 μg of ubiquitin (derived from bovine blood cells) or methylated ubiquitin were incubated with an ubiquitin ligase fraction (Fraction II) from rabbit reticulocytes at 37°C for 2 hours in a buffer containing 50 mmol/L Tris-HCl (pH 9.0), 2 mmol/L ATP, 5 mmol/L $MgCl_2$, and 1 mmol/L dithiothreitol. The conjugation reaction was stopped by boiling the samples in an equal volume of SDS sample buffer followed by separation of the components by SDS–polyacrylamide gel electrophoresis. To examine the ubiquitinated state of α-synuclein, we compared the mobilities of α-synuclein derived from Kii ALS/PDC, ubiquitinated, and unubiquitinated recombinant α-synuclein by SDS–polyacrylamide gel electrophoresis using anti-ubiquitin monoclonal antibody 1510 (anti-Ub 1510) (12). Ubiquitinated and unubiquitinated recombinant α-synuclein were identified by labeling with PSer129 and Syn102.

RESULTS

A representative image of a neuron with LBs and adjacent neurons with NFTs is shown in Figure 1A. Various types of phosphorylated α-synuclein–positive structures, including neuronal cytoplasmic inclusions and LBs (Fig. 1B), Lewy neurites (Fig. 1C), and glial cytoplasmic inclusions (Fig. 1D), were found in all ALS/PDC cases. There were no neuronal intranuclear inclusions. Phosphorylated α-synuclein–positive neurons were found in 8 (80%) of the 10 cases. Phosphorylated α-synuclein–positive neurons were

TABLE 2. Topographical Distribution of α-Synuclein–Positive Neurons and Tau-Positive Neurons

			Case 1	Case 2	Case 3	Case 4	Case 5	Case 6	Case 7	Case 8	Case 9	Case 10
Diagnosis:			ALS	ALS	ALS	ALS With D	ALS With D	PDC	PDC	PDC	PDC	PDC
Sex			F	F	F	M	M	F	F	F	F	M
Age, y			70	63	66	65	77	70	60	76	70	75
Frontal cortex BA8/9		Tau	−	+	+	++	NA	++	+	++	+	−
		αS	−	−	NA	−	−	−	−	−	−	−
Cingulate gyrus BA24		Tau	−	+	NA	+	NA	NA	−	+	++	−
		αS	−	−	NA	−	−	−	−	−	−	−
Insula		Tau	+	++	+	++	+	++	++	+	++	+
		αS	−	−	NA	−	−	−	−	−	−	+
Parietal cortex BA40		Tau	NA	NA	NA	+	NA	NA	NA	+	−	+
		αS	−	−	NA	−	NA	NA	NA	NA	−	±
Temporal cortex BA21		Tau	+	+++	+	+	+++	+++	++	++	++	+
		αS	−	−	−	−	−	−	−	±	−	+
Hippocampus (Ammon horn)		Tau	+++	+++	+	+++	+++	+++	+++	+++	+++	+++
		αS	−	−	−	−	−	−	++	+	−	++
Meynert nucleus		Tau	+	+	NA	++	++	++	+++	NA	+	+
		αS	−	−	NA	−	−	−	+++	NA	−	−
Caudate nucleus		Tau	−	+	NA	+	+	NA	±	+	+	−
		αS	−	−	NA	−	−	−	+	−	+	−
Putamen		Tau	+	++	NA	+	+	NA	±	+	+	+
		αS	−	−	NA	−	−	−	+	−	−	−
Pallidum		Tau	−	+	NA	+	+	NA	±	NA	+	+
		αS	−	−	NA	−	−	−	+	NA	−	−
Transentorhinal cortex BA28		Tau	++	+++	+	++	++	+++	+++	+++	++	+++
		αS	−	−	−	−	−	−	+	++	−	±
Motor cortex		Tau	NA	+	NA	+	+	++	+	+	++	NA
		αS	NA	NA	NA	−	−	−	−	−	−	−
Thalamus		Tau	−	+	+	+	−	NA	++	+	++	+
		αS	−	NA	NA	−	−	NA	−	NA	−	−
Subthalamic nucleus		Tau	−	+	NA	+	NA	NA	NA	+	+	+
		αS	−	NA	NA	−	NA	NA	NA	NA	±	±
Amygdala		Tau	+++	+++	+++	+++	+++	++	+++	++	+++	+++
		αS	−	−	−	+	+	+	++	+	±	+++
Parahippocampus		Tau	+++	+++	+	++	+++	+++	+++	+++	+++	+++
		αS	−	−	−	−	−	−	++	+	−	+++
Cerebellum	Molecular layer	Tau	−	−	−	−	−	−	+	−	−	−
		αS	−	−	−	−	−	−	−	−	−	−
	Dentate nucleus	Tau	−	+	−	+	+	+	++	+	+++	+
		αS	−	−	−	+	−	−	−	+	−	−
	White matter	Tau	−	−	−	−	−	+	−	−	+	−
		αS	−	−	−	−	−	−	−	±	−	−
Midbrain	Substantia nigra	Tau	−	+	+	+	+	++	+	+++	+++	++
		αS	++	−	−	+	−	−	++	+	−	++
	Periaqueductal gray	Tau	+	+++	+++	+++	+	+	++	+++	+++	+++
		αS	+	−	−	+	−	−	+++	++	−	++
Pons	Locus coeruleus	Tau	+	++	+	+	+	+	+	+++	+++	+++
		αS	+++	−	−	+++	−	−	−	+++	−	+++
	Raphe nuclei	Tau	+	+	+	+	+	+	+	+	+++	+++
		αS	−	−	−	+	−	−	−	+++	−	++
	Pontine nucleus	Tau	−	−	−	−	−	−	−	+	+++	−
		αS	−	−	−	−	−	−	−	−	−	−

(Continued on next page)

TABLE 2. *(Continued)*

			Case 1	Case 2	Case 3	Case 4	Case 5	Case 6	Case 7	Case 8	Case 9	Case 10
Diagnosis:			ALS	ALS	ALS	ALS With D	ALS With D	PDC	PDC	PDC	PDC	PDC
Sex			F	F	F	M	M	F	F	F	F	M
Age, y	70		63	66	65	77	70	60	76	70	75	
Medulla	Dorsal nucleus of vagus nerve	Tau	+	+	−	−	−	+	−	−	−	+
		αS	+	−	−	+++	−	−	−	−	−	+++
	Hypoglossal nucleus	Tau	+	±	−	−	−	+	+	−	+	−
		αS	−	−	−	−	−	−	−	−	−	+
	Inferior olivary nucleus	Tau	−	−	−	−	−	+	+	−	+	++
		αS	−	−	−	−	−	−	−	−	−	+
spinal cord	Ventral horn	Tau	−	−	−	NA	−	−	+	+	++	+
		αS	−	−	−	NA	−	−	−	++	−	+
	Intermediolateral nucleus	Tau	−	−	+	NA	−	−	+	+	+	−
		αS	±	−	−	NA	−	−	±	−	−	+++

α-Synuclein (αS)–positive neurons were counted in microscope fields at a magnification of 100× and the density of α-synuclein positive neurons was scored as follows: −, 0; ±, 1; +, 2 to 5; ++, 6 to 10; +++, more than 10. The density of tau-positive neurons was scored at a magnification of 100× as follows: to , 0; +, 1 to 10; ++, 11 to 20; +++, more than 20.

mainly detected in the amygdala (70%); substantia nigra, periaqueductal gray (50%); locus coeruleus (40%); and hippocampus, transentorhinal cortex, parahippocampus, raphe nucleus, dorsal vagal nucleus, and intermediolateral nucleus of the spinal cord (30%) (Table 2). There were no phosphorylated α-synuclein–positive structures in the molecular layer of the cerebellum in any of the 10 cases. Tau-positive neurons were abundant in most areas examined. Phosphorylated α-synuclein–positive neurons outnumbered tau-positive neurons in the substantia nigra, locus coeruleus, and dorsal nucleus of the vagus nerve in a few patients, and periaqueductal gray, raphe nucleus, spinal ventral horn, and spinal intermediolateral nucleus in only 1 or 2 patients (Table 2). Semiquantitative evaluation suggested that the densities of

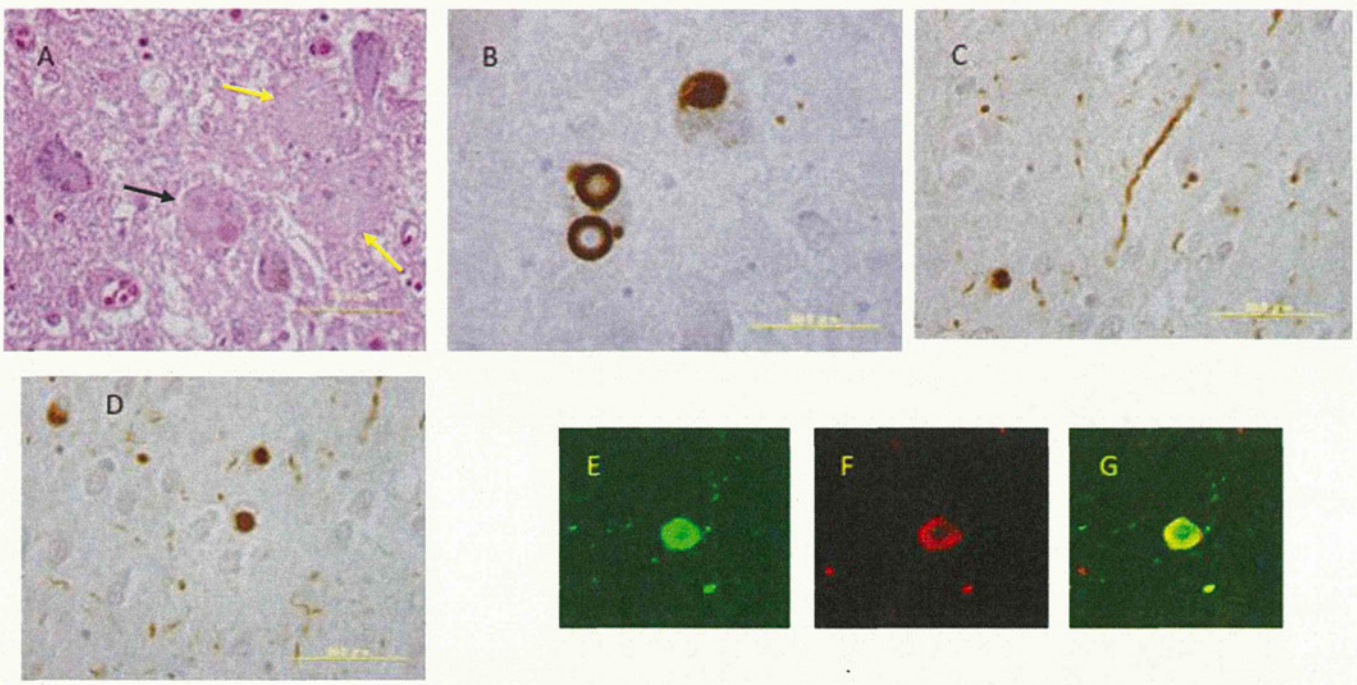

FIGURE 1. Hematoxylin and eosin staining, immunostaining using an antibody against phosphorylated α-synuclein (PSer129), and double immunofluorescence with PSer129 and anti-phosphorylated tau (AT8) antibodies. **(A)** Lewy bodies (LBs) (black arrow) and neurofibrillary tangles (NFTs) (yellow arrows) in the locus coeruleus (hematoxylin and eosin stain). **(B)** LBs and cytoplasmic round inclusion in the locus coeruleus (PSer129). **(C)** Lewy neurites in the amygdala (PSer129). **(D)** Glial cytoplasmic inclusion in the amygdala (PSer129). **(E–G)** Double immunofluorescence labeling showing the coexistence of α-synuclein (PSer129, Alexa 488: green) **(E)**, tau (AT8, Alexa 546: red) **(F)**, and their merged image **(G)**.

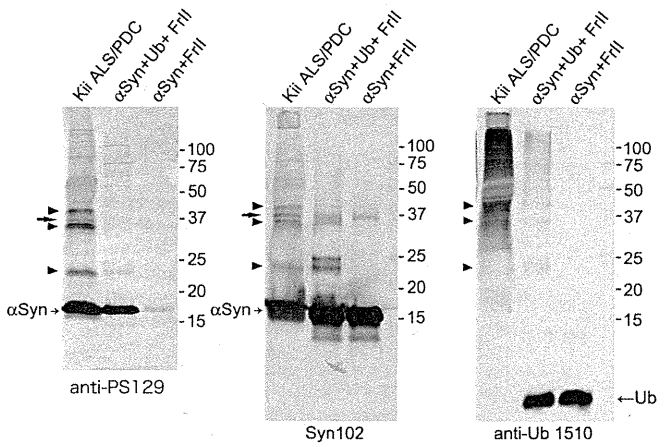

FIGURE 2. Sarkosyl-insoluble fractions from case 10 with Kii amyotrophic lateral sclerosis/parkinsonism dementia complex (ALS/PDC), ubiquitinated recombinant α-synuclein (αSyn + Ub + Frll), and nonubiquitinated recombinant α-synuclein (αSyn + Frll). Samples were immunoblotted with a phosphorylation-dependent anti–α-synuclein antibody (anti-PSer129) (PS129), a phosphorylation-independent anti–α-synuclein antibody (Syn 102), and an anti-ubiquitin (Ub) antibody (anti-Ub 1510). Note that 24-, 32-, and 40-kDa bands are detected in the Kii ALS/PDC brain and αSyn + Ub + Frll with anti-PSer129, Syn 102, and anti-Ub 1510 (arrowheads). Arrow indicates an α-synuclein dimer, which was also detected in αSyn + Frll.

phosphorylated α-synuclein–positive neurons were not related to age or duration of illness but to the densities of tau-positive neurons. Colocalization of phosphorylated α- synuclein and phophorylated tau was observed in many neuronal cytoplasmic inclusions and neuropil threads in the amygdala, substantia nigra, periaqueductal gray, locus coeruleus (Figs. 1E–G), hippocampus, transentorhinal cortex, and parahippocampus.

Immunoblots of sarkosyl-insoluble fractions extracted from the brain of a Kii ALS/PDC patient showed a few α-synuclein–immunoreactive bands. The major immunoreactive band with an apparent molecular mass of 17 kDa and minor 24-, 32-, and 40-kDa bands migrating at a higher molecular mass range on the Tris–glycine gel system were immunoreactive with PSer129 and Syn102. The higher molecular mass of phosphorylated α-synuclein-related polypeptides suggested ubiquitination compared with recombinant α-synuclein, which was incubated with the ubiquitin ligase fraction with or without ubiquitin (Fig. 2), as previously reported in other synucleinopathies (12).

DISCUSSION

α-Synuclein–positive pathology has been identified in a variety of disorders with extensive tau pathology including sporadic Alzheimer disease (13, 14), familial Alzheimer disease (15), DLB (16), familial DLB (17), familial Parkinson disease associated with the α-synuclein A53T mutation (18), Down syndrome (19), neurodegeneration with brain iron accumulation (20–22), and Guam PDC (7–9). Colocalization of tau and α-synuclein was variable in these diseases. For example, extensive colocalization of tau and α-synuclein was reported in DLB (16) and familial DLB (17); the co-occurrence of tau and α-synuclein was variable in Guam PDC (7, 8).

In the present study, the frequency, distribution, and morphology of α-synuclein deposits are described in the brains and spinal cords of patients with Kii ALS/PDC for the first time. α-Synuclein deposits were observed mainly in the limbic system and brainstem; α-synuclein was phosphorylated and ubiquitinated. Tau-positive neurons were more abundant than α-synuclein–positive neurons in most areas examined, and there was extensive colocalization of tau and α-synuclein.

Although Kii ALS/PDC and Guam ALS/PDC share a number of clinical and neuropathologic features, it remains unclear whether they are identical. Yamazaki et al (7) examined α-synuclein–positive intraneuronal inclusions in the motor cortex, medial temporal lobe, and brainstem of 13 patients with Guam PDC using antibodies against non-phosphorylated α-synuclein; they found that 7 (54%) of 13 PDC patients showed α-synuclein–positive inclusions in at least 1 region of the brain. The authors concluded that the amygdala was most affected by α-synuclein pathology, in which α-synuclein was frequently colocalized with tau. Forman et al (8) reported that α-synuclein pathology of the amygdala in Guam ALS/PDC was present in 37% of 19 patients with PDC, but absent in patients with ALS, preclinical PDC, early PDC/ALS, clinical (pathology pending) PDC, PDC/ALS, and control Chamorro patients. The α-synuclein aggregates rarely colocalized within neurons harboring NFTs. On the basis of these findings, the authors suggested a possible interaction between tau and α-synuclein and tau deposits preceding α-synuclein deposits. Sebeo et al (9) reported that numerous α-synuclein–immunoreactive spherical structures in the molecular layer of the cerebellum were observed in 63.6% of Guam PDC patients. These structures were seen exclusively in patients showing α-synuclein pathology in the amygdala, and were much more pronounced in the hemisphere than in the vermis and were associated with Purkinje cells and Bergmann glia cells.

We found that in Kii ALS/PDC, α-synuclein pathology in the amygdala was absent in patients with ALS but was present in ALS patients with dementia and PDC. These results suggest that the α-synuclein pathology in the amygdala may have been induced by tau deposition and may be related to dementia in ALS/PDC. Because α-synuclein inclusions are not found in every brain with other tauopathies, tau in ALS/PDC cases might accelerate α-synuclein aggregation. The combination of misfolded α-synuclein and tau that occurs in ALS/PDC might promote cytotoxic protofibrils and accelerate protein deposits (23). We carefully searched the cerebellum of Kii ALS/PDC patients for similar α-synuclein–positive structures in the molecular layer but failed to find α-synuclein–positive pathology. In general, neuronal cell loss and tau deposits in the molecular layer are exceptional in Kii ALS/PDC. The cause of this discrepancy in α-synuclein pathology in the cerebellum between Guam ALS/PDC and Kii ALS/PDC might be clarified by using the same antibody and identical staining protocols in further studies.

In summary, α-synuclein–positive structures were common in both ALS and PDC and were mainly distributed

in the brainstem and limbic system. The amygdala was the most affected structure in Kii ALS/PDC. The interaction between tau and α-synuclein might modify the pathogenesis of Kii ALS/PDC.

ACKNOWLEDGMENTS

The authors thank Dr T. Iwatsubo, Department of Neuropathology, University of Tokyo, for providing anti–α-synuclein antibody. The authors also thank Hisami Akatsuka for her special technical assistance in tissue preparation for histopathology.

REFERENCES

1. Hirano A, Malamud N, Elizan TS, et al. Amyotrophic lateral sclerosis and parkinsonism-dementia complex on Guam. Further pathologic studies. Arch Neurol 1966;15:35–51
2. Shiraki H, Yase Y. Amyotrophic lateral sclerosis in Japan. In: Vinken PJ, Bruyn GW, Klawans HL, eds. *Handbook of Clinical Neurology.* Amsterdam, the Netherlands: North Holland Publishing Company, 1975:353–419
3. Kuzuhara S, Kokubo Y, Sasaki R, et al. Familial amyotrophic lateral sclerosis and parkinsonism-dementia complex of the Kii peninsula of Japan: Clinical and neuropathological study and tau analysis. Ann Neurol 2001;49:501–11
4. Mimuro M, Kokubo Y, Kuzuhara S. Similar topographical distribution of neurofibrillary tangles in amyotrophic lateral sclerosis and parkinsonism-dementia complex in people living in the Kii peninsula of Japan suggests a single tauopathy. Acta Neuropathol 2007;113:653–58
5. Spillantini M, Schmidt M, Lee V-Y, et al. α-Synuclein in Lewy bodies. Nature 1997;388:839–40
6. Wakabayashi K, Yoshimoto M, Tsuji S, et al. α-Synuclein immunoreactivity in glial cytoplasmic inclusions in multiple system atrophy. Neurosci Lett 1998;249:180–82
7. Yamazaki M, Arai Y, Baba M, et al. α-Synuclein inclusions in amygdala in the brains of patients with the parkinsonism-dementia complex of Guam. J Neuropathol Exp Neurol 2000;59:585–91
8. Forman MS, Schmidt ML, Kasturi S, et al. Tau and α-Synuclein pathology in amygdala of parkinsonism-dementia complex patients of Guam. Am J Pathol 2002;160:1725–31
9. Sebeo J, Hof PR, Perl DP. Occurrence of alpha-synuclein pathology in the cerebellum of Guamanian patients with parkinsonism-dementia complex. Acta Neuropathol 2004;107:497–503
10. Miake H, Mizusawa H, Iwatsubo T, et al. Biochemical characterization of the core structure of alpha-synuclein filaments. J Biol Chem 2002;277:19213–19
11. Fujiwara H, Hasegawa M, Dohmae N, et al. alpha-Synuclein is phosphorylated in synucleinopathy lesions. Nat Cell Biol 2002;4:160–64
12. Hasegawa M, Fujiwara H, Nonaka T, et al. Phosphorylated α-Synuclein is ubiquitinated in α-Synuclein lesions. J Biol Chem 2002;277:49071–76
13. Hamilton RL. Lewy bodies in Alzheimer's disease: A neuropathological review of 145 cases using α-Synuclein immunohistochemistry. Brain Pathol 2000;10:378–84
14. Kazee AM, Han LY. Cortical Lewy bodies in Alzheimer's disease. Arch Pathol Lab Med 1995;119:448–53
15. Lippa CF, Fujiwara H, Mann DM, et al. Lewy bodies contain altered α-Synuclein in brains of many familial Alzheimer's disease patients with mutations in presenilin and amyloid precursor protein genes. Am J Pathol 1998;153:1365–70
16. Iseki E, Togo T, Suzuki T, et al. Dementia with Lewy bodies from the perspective of tauopathy. Acta Neuropathol 2003;105:265–70
17. Clarimon J, Molina-Porcel L, Gomez-Isla T, et al. Early-onset familial Lewy body dementia with extensive tauopathy: A clinical, genetic, and neuropathological study. J Neuropathol Exp Neurol 2009;68:73–82
18. Giasson BI, Forman MS, Higuchi M, et al. Initiation and synergistic fibrillization of tau and alpha-synuclein. Science 2003;300:636–40
19. Lippa CF, Schmidt ML, Lee VM-Y, et al. Antibodies to α-synuclein detect Lewy bodies in many Down's syndrome brains with Alzheimer's disease. Ann Neurol 1999;45:353–57
20. Hayashi S, Akasaki Y, Morimura Y, et al. An autopsy case of late infantile and juvenile neuroaxonal dystrophy with diffuse Lewy bodies and neurofibrillary tangles. Clin Neuropathol 1992;11:1–5
21. Wakabayashi K, Fukushima T, Koide R, et al. Juvenile-onset generalized neuroaxonal dystrophy (Hallervorden-Spatz disease) with diffuse neurofibrillary and Lewy body pathology. Acta Neuropathol 2000;99:331–36
22. Saito Y, Kawai M, Inoue K, et al. Widespread expression of α-Synuclein and tau immunoreactivity in Hallervorden-Spatz syndrome with protracted clinical course. J Neurol Sci 2000;177:48–59
23. Giasson BI, Forman MS, Higuchi M, et al. Initiation and synergistic fibrillization of tau and alpha-Synuclein. Science 2003;300:636–40

Neurobiology of Disease

Regulation of Mitochondrial Transport and Inter-Microtubule Spacing by Tau Phosphorylation at the Sites Hyperphosphorylated in Alzheimer's Disease

Kourosh Shahpasand,[1] Isao Uemura,[2] Taro Saito,[1] Tsunaki Asano,[3] Kenji Hata,[4] Keitaro Shibata,[5] Yoko Toyoshima,[5] Masato Hasegawa,[6] and Shin-ichi Hisanaga[1]

[1]Laboratory of Molecular Neuroscience, [2]Laboratory of Developmental Program, [3]Laboratory of Cell Genetics, [4]Laboratory of Plant Ecology, Department of Biological Sciences, Tokyo Metropolitan University, Minami-osawa, Hachioji, Tokyo 192-0397, Japan, [5]Department of Life Sciences, Graduate School of Arts and Sciences, The University of Tokyo, Komaba, Tokyo 153-8902, Japan, and [6]Tokyo Metropolitan Institute of Medical Sciences, Department of Neuropathology and Cell Biology, Setagaya-Ku, Tokyo 156-0057, Japan

The microtubule-associated protein Tau is a major component of the neurofibrillary tangles that serve as a neuropathological hallmark of Alzheimer's disease. Tau is a substrate for protein phosphorylation at multiple sites and occurs in tangles in a hyperphosphorylated state. However, the physiological functions of Tau phosphorylation or how it may contribute mechanistically to Alzheimer's pathophysiology are not completely understood. Here, we examined the function of human Tau phosphorylation at three sites, Ser199, Ser202, and Thr205, which together comprise the AT8 sites that mark abnormal phosphorylation in Alzheimer's disease. Overexpression of wild-type Tau or mutated forms in which these sites had been changed to either unphosphorylatable alanines or phosphomimetic aspartates inhibited mitochondrial movement in the neurite processes of PC12 cells as well as the axons of mouse brain cortical neurons. However, the greatest effects on mitochondrial translocation were induced by phosphomimetic mutations. These mutations also caused expansion of the space between microtubules in cultured cells when membrane tension was reduced by disrupting actin filaments. Thus, Tau phosphorylation at the AT8 sites may have meaningful effects on mitochondrial movement, likely by controlling microtubule spacing. Hyperphosphorylation of the AT8 sites may contribute to axonal degeneration by disrupting mitochondrial transport in Alzheimer's disease.

Introduction

Mitochondrial transport within axons is crucial for axonal maintenance, and its dysregulation can contribute to neurodegenerative diseases (Su et al., 2010). In axons, mitochondrial movement is driven by two oppositely directed motor proteins, kinesin and dynein, along microtubules (MTs) (Hollenbeck and Saxton, 2005; Bereiter-Hahn and Jendrach, 2010). The surface of MTs is decorated with microtubule-associated proteins (MAPs) (Marx et al., 2006; Vershinin et al., 2007). Tau serves as a predominant MAP in axons and is a filamentous protein of 441 amino acid residues (the longest human isoform). Tau is comprised of two functional regions, the N-terminal projection domain that protrudes from the surface of MTs and the C-terminal MT-binding domain. Overexpression of Tau inhibits mitochondrial transport in various cells (Ebneth et al., 1998; Trinczek et al., 1999; Stamer et al., 2002; Dixit et al., 2008; Stoothoff et al., 2009; Vossel et al., 2010). However, the mechanism and regulation of Tau-mediated inhibition of mitochondrial transport are not understood.

Tau is a major component of neurofibrillary tangles found in Alzheimer pathology. Tau is also a phosphoprotein, the functions of which can be regulated by phosphorylation (Stoothoff and Johnson, 2005; Hanger et al., 2009). Many of the phosphorylation sites reside in proline-directed (Ser/Thr)-Pro sequences. These sites are moderately phosphorylated in healthy neurons. However, hyperphosphorylation is linked to neurodegeneration with phosphorylation of more than 20 sites shown in the degenerated brains of Alzheimer's patients (Watanabe et al., 1993; Morishima-Kawashima et al., 1995; Stoothoff and Johnson, 2005). Cdk5 and GSK3β are two proline-directed protein kinases that are known to phosphorylate these (Ser/Thr)-Pro sites (Ishiguro et al., 1992; Planel et al., 2002). Furthermore, hyperactivation of Cdk5 or GSK3β reduces mitochondrial movement (Darios et al., 2005; Morel et al., 2010). However, it has not been clearly demonstrated whether Tau is a major downstream target of these kinases and, if so, which phosphorylation site(s) is critical. Among GSK3β- and Cdk5-related phosphorylation sites, Ser199, Ser202, and Thr205 are particu-

Received Nov. 29, 2011; accepted Dec. 12, 2011.

Author contributions: K. Shahpasand and S.-i.H. designed research; K. Shahpasand performed research; I.U., T.S., T.A., K. Shibata, Y.T., and M.H. contributed unpublished reagents/analytic tools; K. Shahpasand, I.U., T.S., K.H., and S.-i.H. analyzed data; K. Shahpasand and S.-i.H. wrote the paper.

This work was supported by Grants-in-Aid for Scientific Research on Priority Area from MEXT of Japan (S.H). K. S. was supported by JGC-S Scholarship Foundation. We thank Dr. Peter Davies at Albert Einstein College of Medicine for providing MC-1 and Alz-50 monoclonal anti-Tau antibodies. We also thank Miss. Elizabeth Zielinska for reading this paper.

Correspondence should be addressed to either Kourosh Shahpasand or Shin-ichi Hisanaga. Laboratory of Molecular Neuroscience, Department of Biological Sciences, Tokyo Metropolitan University, Minami-osawa 1-1, Hachioji, Tokyo 192-0391, Japan. E-mail: kourosh-shahpasand@ed.tmu.ac.jp or hisanaga-shinichi@tmu.ac.jp.

DOI:10.1523/JNEUROSCI.5927-11.2012

 0270-6474/12/322430-12$15.00/0

larly interesting. These phosphorylated sites are recognized by the phosphorylation-dependent monoclonal antibody AT8 (Goedert et al., 1995; Wang et al., 2006; Hanger et al., 2009), and their detection by this antibody is commonly used as a marker of abnormal phosphorylation in brains of Alzheimer's patients. These sites are located at the border of the projection domain and MT-binding Pro-rich region (see Fig. 1*A*). Phosphorylation at these sites may extend the projection domain outwards from the surface of MTs (Jeganathan et al., 2008) and affect mitochondrial transport (Mukhopadhyay and Hoh, 2001; Jeganathan et al., 2008; Shahpasand et al., 2008).

Here, we directly examined the effect of phosphorylation at the AT8 sites on mitochondrial transport using the nonphosphorylatable Ala mutant (3A) and the constitutive phosphorylation mimic Asp mutant (3D) of Tau. Overexpression of Tau 3D decreased the mitochondrial movement and expanded the inter-MT spacing more than that of wild-type (WT) Tau or Tau 3A. These results suggest that phosphorylation at the AT8 sites affects mitochondrial transport by changing the spaces between MTs.

Materials and Methods

Anti-human Tau (A0024) was obtained from Dako. Anti-phospho-Tau antibody AT8 was purchased from Thermo Scientific. Anti-TOM20 (FL-145) was from Santa Cruz Biotechnology. MC-1 and Alz-50 anti-Tau antibodies were generous gifts from Dr. Peter Davies (Albert Einstein College of Medicine, Bronx, NY). Anti–β-tubulin and latrunculin B were from Sigma-Aldrich. Anti-His tag was from Invitrogen. NGF and Phos-tag acrylamide was obtained from Wako Chemicals.

Construction of expression vectors for Tau proteins. Mutations of Tau at Ser199, Ser202, and Thr205 were introduced in the longest wild-type human Tau in a pSG5 expression vector. Double Ala mutants (2A) at Ser202A and Thr205A were constructed with PCR using primers 5′-GGCGCCCCAGG CGCTCCCGGCAGCCGC-3′ (forward) and 5′-CCGCGGGGTCCGC-GAGGGCCGTCGGCG-3′ (reverse). For Tau 3A, an additional Ala mutation at Ser199 was constructed with PCR using Tau 2A as a template and primers 5′-AGCGGCTACAGCGCCCCCGGCGCCCCA-3′ (forward) and 5′-TCGCCGATGTCGCGGGGGCCGCGGGGT-3′ (reverse). Tau 3D was constructed by one-step PCR using Tau 3A as a template and primers 5′-AGCGGCTACAGCGACCCCGGCGACCCAGGCGATCCCGGCAGC-CGC-3′ (forward) and 5′-TCGCCGATGTCGCTGGGGCCGCTGGGTCC GCTAGGGCCGTCGGCG-3′ (reverse). All constructs were confirmed by DNA sequencing. Bacterial expression vectors encoding Tau 3A and Tau 3D were constructed similarly with PCR using Tau 1N4R (one N-terminal insertion and four MT-binding repeats) in the pRK172 vector. Baculovirus expression vectors for Tau proteins were constructed as follows. Tau WT, 3A, or 3D in pSG5 was amplified with PCR using primers 5′-GGATCCATG-GCTGAGCCCCGCCA-3′ (forward, with BamHI site) and 5′-GCGGC-CGCTCACAAACCCTGCTT-3′ (reverse, with NotI site). PCR products were inserted into the pCR2.1 vector. Tau cDNAs were digested with BamHI and NotI and inserted into pFastBac Dual, the donor vector for the Bac-to-Bac Baculovirus Expression System (Invitrogen). Recombinant plasmids were used to transform competent DH10Bac cells for transposition to the bacmid shuttle vectors. Recombinant bacmid DNA was transfected into monolayers of Sf9 insect cells. Supernatants containing virus were harvested 96 h after transfection, and the viral titer was amplified and determined according the manufacturer's instructions (Invitrogen).

Cell culture and expression of Tau proteins. COS-7 cells (2×10^5 per ml) were grown in DMEM (Sigma) containing 10% FBS and transfected with PolyFect reagent (Qiagen) (Kaminosono et al., 2008).

PC12 cells (2×10^5 per ml) were cultured on 35 mm glass-bottom dishes in DMEM containing 10% FBS and antibiotics (penicillin and streptomycin) at 37°C in 5% CO_2. Cells were treated with NGF (50 ng/ml) 4 h after transfection for 3 d.

Primary neurons were prepared from 17-day-old embryonic mouse brain cerebral cortex of either sex. Neurons (2×10^5 per ml) were seeded on 35 mm glass-bottom dishes. The medium was then changed to neurobasal medium supplemented with B27 (Invitrogen) and 1 mM L-glutamine (Endo et al., 2009). Cells were transiently transfected with Tau WT, 3A, or 3D with Lipofectamine 2000 (Invitrogen). Various amounts of Tau cDNA (1–4 μg) were tested to determine the appropriate amount of cDNA. The levels of Tau expression were quantified by immunostaining intensity as described below. Neurons were cotransfected with Mito-GFP to label and observe mitochondrial movement.

Sf9 cells were grown at 27°C in 35 mm dishes in complete serum-free medium (Invitrogen) and antibiotics (penicillin and streptomycin). Monolayer cultures of Sf9 cells (4×10^5 per ml) were infected with baculoviruses encoding Tau cDNA at a titer of 2×10^7 pfu/ml. Cells were treated with 0.5 μg/ml latrunculin B from the time of infection for 72 h and were fixed with 2.5% glutaraldehyde and 2% PFA in PEM buffer (0.1 M PIPES, pH 7.2, 1 mM EGTA, 1 mM $MgCl_2$) for 30 min at room temperature.

Immunostaining. One day after transfection, COS-7 cells were treated with PEM buffer containing 4 M glycerol and 0.5% Triton X-100 for 10 min at 37°C. After fixation with cold methanol for 3 min, cells were incubated with anti-tubulin (1:500) or anti-Tau (1:500), followed by Alexa Fluor-conjugated anti-mouse IgG or anti-rabbit IgG (1:500).

Sf9 cells, PC12 cells, and cortical neurons cultured on glass coverslips were fixed with 4% PFA in PBS for 20 min and permeabilized with 0.1% Triton X-100 in PBS containing 5% BSA for 20 min. Cells were incubated with anti-Tau (1:500) followed by Alexa Fluor 546-labeled secondary antibody. Immunofluorescent stainings were examined with an LSM5 EXCITER microscope (Zeiss), and fluorescent intensities were measured for 20 processes per sample with ZEN 2008 software (Zeiss). Length and width of Sf9 cell processes were measured for 20 cells per sample with ImageJ software.

Electron microscopy. Sf9 cells were infected with baculovirus encoding Tau constructs and 72 h after infection cells were fixed and processed for electron microscopic observation (Tokuoka et al., 2000). PC12 cells were transfected with plasmids encoding Tau and EGFP. Tau-expressing PC12 cells were identified with EGFP after fixation, and their positions were marked on the base of culture dishes by a felt pen. Fixation was done with 2.5% glutaraldehyde and 2% PFA in PEM buffer (0.1 M PIPES, pH 7.2, 1 mM EGTA, 1 mM $MgCl_2$) for 30 min at room temperature. Specimens were examined with a JEM-1010 transmission electron microscope (JEOL). Inter-MT distances in sections cut perpendicularly to longitudinal axis of MTs were measured with ImageJ software.

Time-lapse imaging and statistical methods. Mitochondrial movement in NGF-treated PC12 cells and mouse brain cortical neurons was examined with an LSM 5 EXCITER microscope using an incubation chamber with 5% CO_2 at 37°C. Fluorescent images of mitochondria in the longest process of each PC12 cell and axons of cortical neurons were acquired at intervals of 5 s over a period of 300 s. In each experiment, eight mitochondria in five cells were analyzed for their movement in image stacks composed of 60 images. Individual mitochondrial movements were analyzed with ZEN 2008 software (Zeiss). Differences in the position of each mitochondrion between two frames during each 5 s interval were exported to Excel, and they were classified and scored as stationary, anterograde, or retrograde movements. Completely immotile mitochondria during 300 s of observation were excluded from the counts. Kymographs were made using serial frames of the same area during the observation period.

Statistical differences in stationary phase of mitochondria among control, Tau WT, 3A, and 3D were analyzed by one-way ANOVA. Holm's multiple test was conducted on all possible pairwise combinations. Differences in the ratios between anterograde and retrograde movements were analyzed by ANCOVA. The dependent variable was time of anterograde movement, and the independent variables were Tau transfection samples as a fixed factor and time of retrograde movement as a covariate. After confirming no interaction between Tau transfection samples and the retrograde ratios, the anterograde/retrograde moving durations were compared using all data or data of Tau-transfected samples. When $p > 0.05$, the difference was considered nonsignificant. All of the statistical analyses were carried out with version 2.13.1 of the R software package (R: A language and environment for statistical computing. R Development Core Team, Vienna, Austria, 2011, available at http://www.R-project.org).

Protein purification, motor–MT binding assay, and in vitro *phosphorylation of Tau by Cdk5-p25.* Tau WT, 3A, or 3D was expressed in *Escherichia coli* and purified (Sakaue et al., 2005). Porcine brain tubulin was also purified as described (Sakaue et al., 2005). Kinesin RK430-AviTag-KRC-His_6 was expressed and purified from *E. coli* as described (Furuta et al., 2008), except that ATP was not added to the preparation buffers. Tubulin (0.5 μM) was assembled in PEM containing 1 mM GTP and 10 μM Taxol in the presence of various concentrations of Tau WT, 3A, or 3D (0.05, 0.1, or 0.15 μM) and 0.1 μM RK430 at 37°C for 45 min. Polymerized MTs were collected by centrifugation at 100,000 × *g* for 60 min at 37°C. The supernatants and pellets were subjected to SDS-PAGE followed by immunoblotting. Cdk5-p25 was purified from Sf9 cells that had been infected with baculovirus encoding Cdk5 and p25 (Saito et al., 2003). Phosphorylation of Tau by Cdk5-p25 was performed *in vitro* by incubating 50 μg/ml Tau WT, 3D, or 3A with Cdk5-p25 at 37°C for 2 h.

SDS-PAGE and immunoblotting. SDS-PAGE and immunoblotting were performed as described (Sakaue et al., 2005). Phos-tag SDS-PAGE was performed with 7.5% polyacrylamide and 50 μM Phos-tag as described (Hosokawa et al., 2010). Dot blot was performed with MC-1 and Alz-50 antibodies using the method reported previously (Jicha et al., 1997). All experiments were performed at least three times, and representative results are shown.

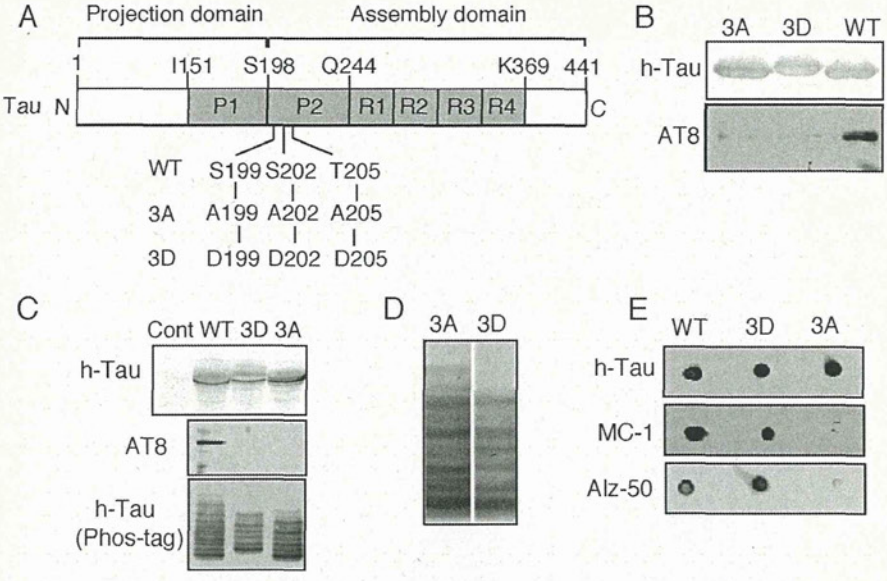

Figure 1. Phospho-mimic mutant of Tau 3D at the AT8 sites Ser199/Ser202/Thr205. ***A***, Schematic representation of the longest human isoform of Tau composed of 441 amino acid residues. Tau consists of the N-terminal projection domain and C-terminal MT-assembly domain including four MT-binding repeats (R1–R4). Two proline-rich regions (P1 and P2) are present in the middle region. The AT8 Ser199/Ser202/Thr205 sites are located in the N-terminal side of P2 at the border of the projection domain and MT-binding domain. This molecular structure was drawn based on the description by Jeganathan et al. (2006). Amino acids that can be phosphorylated were replaced with Asp or Ala to generate the phosphorylation mimic (3D) or nonphosphorylated (3A) Tau constructs, respectively. ***B***, Cdk5-dependent *in vitro* phosphorylation at the AT8 sites of Tau WT, but not Tau 3A or 3D. Tau WT, 3A, and 3D were phosphorylated *in vitro* with Cdk5–p25. Immunoblots were performed with anti-human Tau (h-Tau) or AT8. ***C***, Phosphorylation at the AT8 sites of Tau WT, but not 3A or 3D, in COS-7 cells. Tau WT, 3A, or 3D was expressed in COS-7 cells. Cell lysates were subjected to immunoblotting for h-Tau or AT8. The bottom panel shows evaluation of phosphorylation state-dependent mobility shifts of Tau WT, 3A, or 3D expressed in COS-7 cells by Phos-tag SDS-PAGE. Tau WT, 3A, and 3D separated by Phos-tag SDS-PAGE were immunoblotted with anti-human Tau. Cont, Control. ***D***, Alignment of Tau 3A and 3D to compare their banding patterns in Phos-tag SDS-PAGE. Phos-tag immunoblots of Tau 3A and 3D in ***C*** were aligned by adjusting the fastest moving band. ***E***, Tau 3D takes conformation similar to phosphorylated Tau WT. After *in vitro* phosphorylation of Tau constructs with Cdk5–p25, dot blots were performed with phosphorylation-independent antibody h-Tau (top) and with phosphorylation-dependent antibodies, MC-1 (middle), and Alz-50 (bottom).

Results

Phosphorylation of Tau mutants and their binding to MTs

Tau can be phosphorylated at multiple sites *in vitro* and *in vivo*. To assess the effects of site-specific phosphorylation on mitochondrial transport, we used the Tau mutants 3A (nonphosphorylatable) and 3D (phosphorylation mimic), each of which was mutated at the AT8 Alzheimer phosphorylation sites (Ser199, Ser202, and Thr205) (Fig. 1*A*). Recombinant Tau WT, 3A, and 3D were phosphorylated *in vitro* by Cdk5-p25 and immunoblotted with AT8, which recognizes Tau that is phosphorylated at Ser202 and Thr205 (Goedert et al., 1995) or Ser199, Ser202, and Thr205 (Hanger et al., 2009). Phosphorylated Tau WT was immunoreactive to AT8, whereas phosphorylated Tau 3A and 3D were not (Fig. 1*B*), confirming that Cdk5 indeed phosphorylated the sites recognized by AT8 (Takahashi et al., 2003) and that these phosphorylation sites were disrupted in 3A and 3D constructs. These Tau constructs were expressed in COS-7 cells, and phosphorylation was examined by immunoblotting with AT8. Immunodetection of Tau WT but not 3A nor 3D clearly demonstrated that Tau WT was phosphorylated at the AT8 recognition sites in COS-7 cells (Fig. 1*C*, middle).

To determine whether the mutations affected phosphorylation of Tau at other sites, Tau expressed in COS-7 cells was detected by immunoblotting with a phosphorylation-independent Tau antibody after Phos-tag SDS-PAGE. Phos-tag SDS-PAGE is a recently developed method that detects phosphorylated proteins via an expanded mobility shift on SDS-PAGE (Kinoshita et al., 2006; Hosokawa et al., 2010). Multiple Tau bands indicated the presence of various phosphorylated forms of Tau in COS-7 cells (Fig. 1*C*, bottom). As a whole, the decreased mobility of Tau WT compared to Tau 3A indicated the higher level of phosphorylation of Tau WT, including the AT8 site. The relative upward shift of all the Tau 3D bands was apparently due to the increased negative charge of the three Asp residues at positions 199, 202, and 205. Phosphorylated Tau 3A and 3D had similar, but not identical, banding patterns, suggesting that these mutants underwent similar phosphorylation at other sites (Fig. 1*D*). These results indicated that by using Tau 3A and 3D, we could examine the role of Tau phosphorylation at the AT8 sites (Ser199/Ser202/Thr205) on mitochondrial transport.

To see whether the 3D mutant mimics the phosphorylation state at the AT8 sites, we performed dot blot of Tau constructs with MC-1 and Alz-50 antibodies after phosphorylation with Cdk5-p25. MC-1 and Alz-50 are monoclonal antibodies that recognize conformation of Tau when phosphorylated at both AT8 and PHF-1 (Ser396 and Ser 404) sites (Jicha et al., 1999). Cdk5-phosphorylated Tau WT and Tau 3D, but not Tau 3A, were immunoreactive to MC-1 and Alz-50 (Fig. 1*E*). The results indicated that Tau 3D in fact mimics phosphorylation at the AT8 sites.

To assess Tau 3A and 3D binding to MTs, COS-7 cells were transfected with vectors that mediated expression of WT, 3A, or 3D forms of Tau. The Tau-expressing cells were then incubated in a MT-stabilizing buffer containing 0.5% Triton X-100 and 4 M glycerol to remove soluble tubulin and Tau and then stained with anti-tubulin and anti-Tau (Bershadsky et al., 1978; Kaminosono

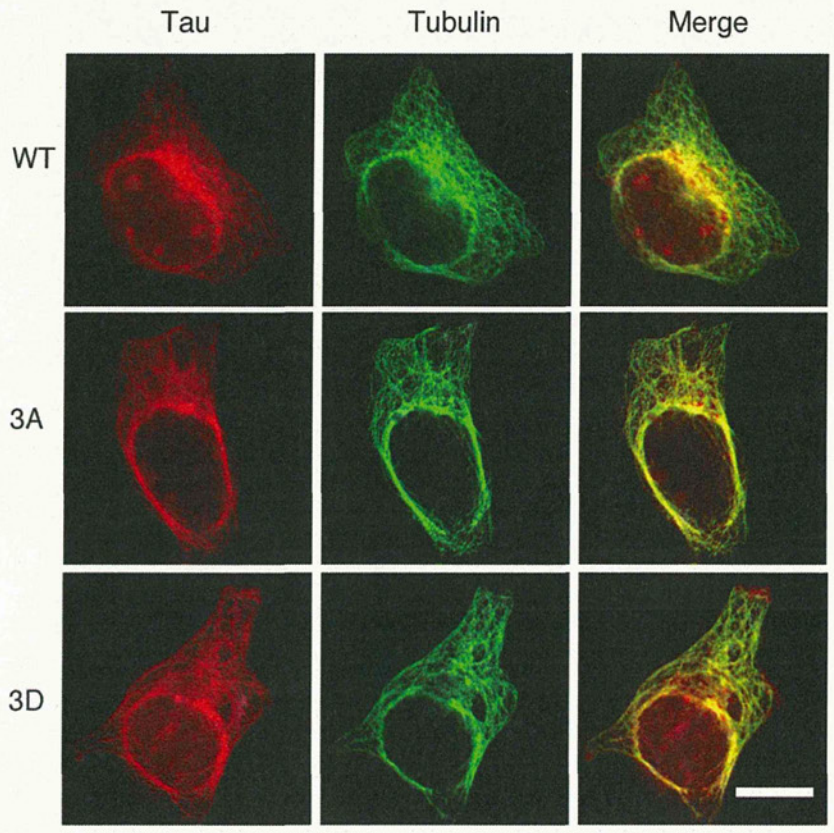

Figure 2. Colocalization of Tau WT, 3A, or 3D to MTs in COS-7 cells. Tau WT, 3A, or 3D vectors were used to transfect COS-7 cells. Soluble Tau and tubulin were removed by treatment with PEM containing 4 M glycerol and 0.5% Triton X-100 for 10 min at 37°C, and cells were double-stained with anti-tubulin (green in middle panels) and anti-Tau (red in left panels), followed by fluorescently labeled secondary antibodies. Merged images are shown in the right panels. Scale bar, 20 μm.

et al., 2008). In all three cases, there was wide codistribution of Tau and MT (Fig. 2), suggesting that Tau phosphorylation at the AT8 sites does not inhibit the binding of Tau to MTs in cells, as reported previously (Rankin et al., 2005; Hanger et al., 2009). Furthermore, *in vitro* studies indicated that both recombinant pure Tau 3A and 3D bound to MTs similarly to Tau WT (data not shown).

Expression of Tau constructs in PC12 cells and cultured cortical neurons

Expression levels of Tau WT, 3A, and 3D in PC12 cells and cultured neurons were measured after immunofluorescent staining. The immunostainings of neurons are shown in Figure 3*A*. The staining intensity increased with concentrations of plasmids from 2 to 3 μg used for transfection (Fig. 3*B*,*C*). When 2.5 μg of plasmids were used, the fluorescent intensities were ~1.7 and ~1.5 fold of untransfected PC12 cells (Fig. 3*B*) and cultured neurons (Fig. 3*C*), respectively. Expression levels were almost similar among Tau WT, 3A, and 3D constructs (Fig. 3*B*,*C*). The effect of Tau on mitochondrial movement was dependent on the amount of Tau plasmid used for transfection. While transfection with less than 2 μg did not significantly affect mitochondrial movement, more than 3 μg had a substantial (and similar) effect for all Tau constructs (data not shown). Differences were observed with 2.5 μg DNA, which was used in subsequent experiments.

Tau phosphorylation reduces mitochondrial motility in neuritic processes of PC12 cells

To determine the effect of Tau mutants on mitochondrial movement in parallel bundles of MTs, we first used NGF-treated PC12 cells, which have been previously employed for MT-mitochondria studies (Tatebayashi et al., 2004; Morel et al., 2010). We cotransfected Tau constructs and Mito-GFP into PC12 cells and observed the movement of GFP-labeled mitochondria in neurite-like processes 3 d after NGF treatment. Mitochondria were distributed throughout the processes of PC12 cells (left panels of Fig. 4*A*). Mitochondrial motility was recorded over 300 s in randomly selected processes, and examples are shown as kymographs in Figure 4*A*. The number of motile mitochondria was higher in control PC12 cells compared with Tau-overexpressing cells. The percentages of stationary phase of mitochondria, direction of movement, and velocity were quantified (Fig. 4*B–D*). The ratio of stationary phase was 23.0% in control PC12 cells but 47.6% in cells expressing Tau WT and 44.1% for 3A; for 3D, however, the percentage was higher still, 61.3% (Fig. 4*B*). Moving mitochondria in neurites overexpressing Tau 3D were significantly fewer than those in Tau WT or 3A-expressing neurites, indicating the stronger inhibitory activity of Tau 3D. Effect of Tau overexpression on anterograde and retrograde movements is shown in Figure 4*C*. Overexpression of each Tau construct specifically decreased the anterograde movement of mitochondria (compare control with WT/3A/3D in Fig. 4*C*). However, neither Tau 3D nor 3A had further preferential effect on the direction of mitochondrial movement (Fig. 4).

Tau overexpression also affected the velocity of mitochondrial movement in both directions. In control PC12 cells, the velocity was normally distributed with a peak at 0.2–0.3 μm/s (Fig. 4*D*). The mean velocities were around 0.29 ± 0.03 and 0.31 ± 0.04 μm/s for anterograde and retrograde movement, respectively. Tau overexpression shifted the peak to <0.1 μm/s. The percentages of the total anterograde- and retrograde-moving mitochondria moving <0.1 μm/s were 53.3 and 57.7% in Tau WT-expressing PC12 cells, 54.2 and 62.6% in Tau 3A–expressing PC12 cells, and 54.3 and 56.8% in Tau 3D-expressing PC12 cells, respectively. The mean velocities for anterograde and retrograde movement were reduced to 0.19 ± 0.056 and 0.17 ± 0.035 μm/s by Tau WT overexpression, 0.20 ± 0.02 and 0.17 ± 0.07 μm/s by Tau 3A overexpression, and 0.22 ± 0.06 and 0.18 ± 0.04 μm/s by Tau 3D overexpression, respectively. Notably, for Tau 3D there was a second peak of mitochondrial movement with a velocity of ~0.4–0.6 μm/s, particularly in the anterograde direction. Thus, there may be a population of mitochondria that is less affected by Tau 3D. The results that Tau overexpression increased the stationary phase of mitochondria are consistent with previous reports (Trinczek et al., 1999; Thies and Mandelkow, 2007; Stoothoff et al., 2009). Our novel finding was that phosphorylation mimic mutation (3D) at the AT8 Alzheimer sites had an additional effect on mitochondrial motility compared with Tau WT and 3A in neuron-like processes of PC12 cells.

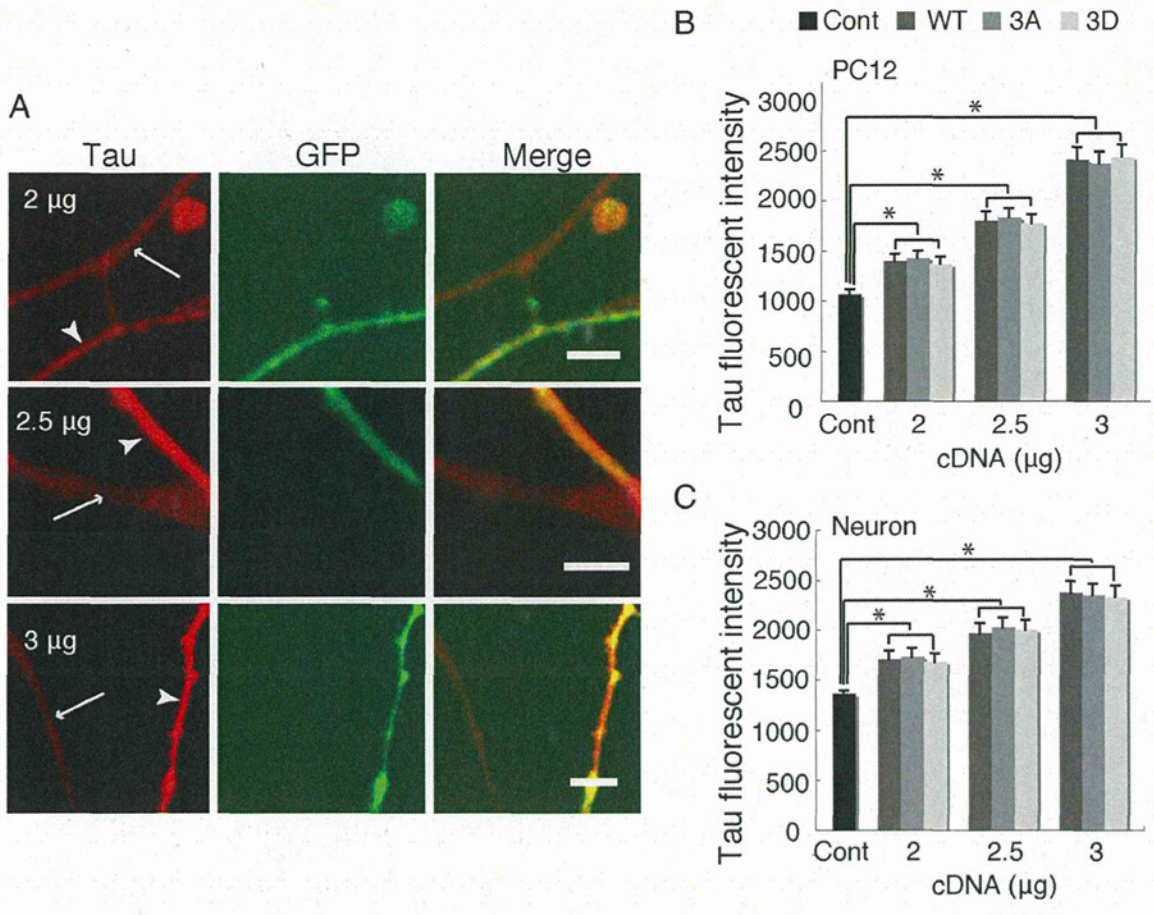

Figure 3. Quantification of levels of Tau overexpression in the PC12 cell neurites and in neuronal axons. ***A***, Immunostaining of cortical neurons overexpressing Tau with anti-human Tau. Plasmids encoding Tau at concentrations of 2, 2.5, and 3 μM were cotransfected with EGFP vector into cultured cortical neurons at DIV6, and these neurons were stained at DIV11. Transfected axons are indicated with arrowheads and un-transfected axons with arrows. Scale bar, 5 μm. ***B***, ***C***, Quantification of Tau expressed in PC12 cell neurites (***B***) and axon of cortical neurons (***C***). ($n = 20$ for each of PC12 cells and neurons, $^*p < 0.01$, one-way ANOVA). Cont, Control.

Increased pausing and decreased velocity of mitochondria in axons of cultured neurons expressing Tau 3D

Tau is predominantly expressed in neuronal axons. We therefore compared the effects of Tau 3D with those of Tau WT or 3A on mitochondrial movement in axons of cultured cortical neurons. Mitochondrial distribution in axons transfected with Tau and Mito-GFP are shown in left panels of Figure 5*A*. During the 300 s observation period, mitochondria exhibited complex motile behavior such as anterograde and retrograde movements with frequent pausing. The duration of stationary phase was 31.6% in control neurons, which was higher than that observed in PC12 cells, consistent with a previous report (Morel et al., 2010). A significant increase in stationary phase was observed after transfection with Tau WT (48.5%) or 3A (46.6%); however, a higher stationary state (64.4%) was caused by Tau 3D (Fig. 5*B*). The stational phase induced by Tau 3D was significantly higher than those induced by Tau WT and 3A, indicating that Tau 3D has stronger inhibitory activity against mitochondrial movement. Direction-dependent inhibition of mitochondrial movement by Tau is summarized in Figure 5C. Tau protein dramatically reduced the population of anterograde-moving mitochondria, consistent with previous reports (Stamer et al., 2002; Dixit et al., 2008; Vershinin et al., 2008; Stoothoff et al., 2009). However, the ratio of mitochondria moving anterogradely and retrogradely was not different among three Tau constructs, indicating that phosphorylation at the AT8 sites does not affect the direction of mitochondrial movements.

Tau overexpression also reduced the velocity of mitochondria in axons. In control neurons, mitochondria showed a peak velocity of 0.2–0.3 μm/s in both directions, and a substantial proportion also moved faster than 0.6 μm/s (Fig. 5*D*). Tau overexpression shifted the peak to a slower rate, with peak velocities of 0.05–0.3 μm/s, depending on the Tau construct. The relative ratio of mitochondria with velocities less than 0.3 μm/s in the anterograde and retrograde directions were 31.0 and 38.2% in control neurons, 88.3 and 84.4% in Tau WT-expressing neurons, 86.9 and 82.6% in Tau 3A-expressing neurons, and 84.7 and 84.4% in Tau 3D-expressing neurons. The mean anterograde and retrograde velocities were 0.55 ± 0.08 and 0.45 ± 0.03 μm/s, respectively, in control cells, but they were reduced to 0.17 ± 0.03 and 0.18 ± 0.06 μm/s in Tau WT-overexpressing neurons, 0.18 ± 0.03 and 0.19 ± 0.07 μm/s in Tau 3A-overexpressing neurons, and 0.18 ± 0.03 and 0.18 ± 0.04 μm/s in Tau 3D-overexpressing neurons. Velocities faster than 1 μm/s, which accounted for 15 and 11% of anterograde and retrograde movements, respectively, in control neurons, were not observed in any Tau-overexpressing neurons. As in PC12 cells, neurons expressing Tau 3D had a small proportion of mitochondria that moved at ~0.5–0.6 μm/s, particularly in the anterograde direction, whereas neurons expressing Tau WT or 3A did not. Thus, Tau with phosphorylation mimic mutation (3D) at the AT8 sites suppressed mitochondrial movement in axons of cultured cortical neurons more than Tau WT or 3A.

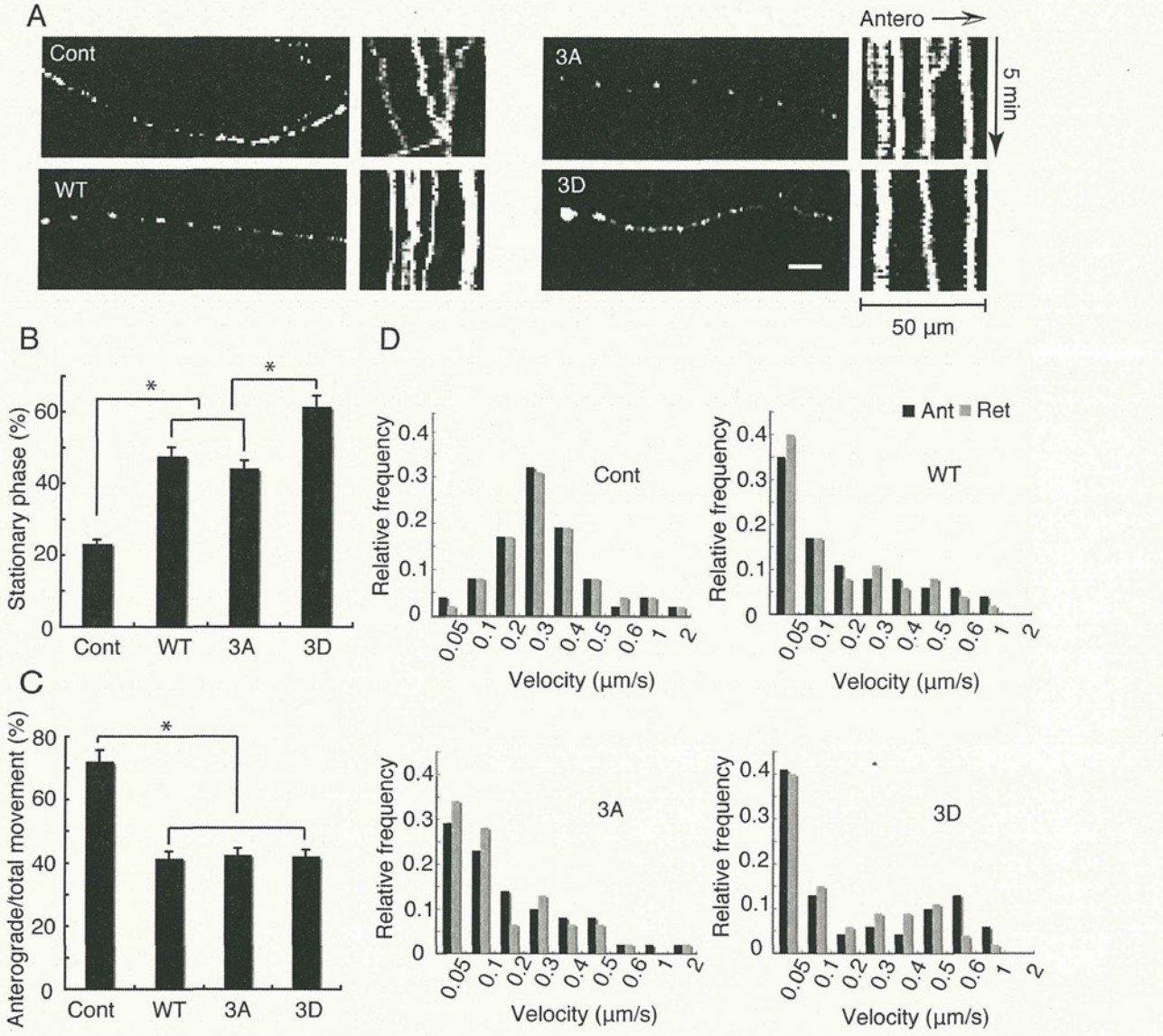

Figure 4. Effects of Tau WT, 3D, or 3A on mitochondrial movement in PC12 cells. ***A***, Mitochondrial distribution and movements in neurite process of PC12 cells. PC12 cells were transfected with a Mito-GFP vector alone as a control (Cont) or cotransfected with a Mito-GFP and Tau WT, 3A, or 3D vector. PC12 cells were treated with NGF for 72 h after transfection. Mitochondrial distribution is shown by fluorescence of Mito-GFP (left panels). Right panels are kymographs of mitochondria moving in a process of a PC12 cell. Antero, Anterograde. Bar, 20 μm. ***B***, The percentage ratio of pausing mitochondria in PC12 cell processes. Mitochondrial movement was recorded in the neurite-like processes at 5 s intervals over a 300 s period. Any mitochondrion that translocated at least 0.1 μm between two image frames was considered to be moving. The pausing time was expressed as the percentage of the total observation time ($n = 35$, $^*p < 0.01$, one-way ANOVA). ***C***, Effect of Tau WT, 3A, or 3D on anterograde or retrograde movement of mitochondria. The vertical axis indicates the ratio of anterogradely moving time to total moving duration. Statistical analysis was performed by ANCOVA as described in Materials and Methods. The ratio was significantly different between control and Tau-overexpressing PC12 cells ($^*p < 0.01$), but was not significant between three Tau constructs ($p = 0.75$). ***D***, Effect of Tau WT, 3D, or 3A on the velocity of mitochondria. Relative frequency of mitochondria moving at the indicated velocities in the anterograde (Ant, black) or retrograde (Ret, gray) direction for control, WT, 3A, or 3D. $n = 35$ mitochondria per sample.

The binding of kinesin to MTs is not affected by Tau in any phosphorylation state

Tau impairs mitochondrial movement by inhibiting the interaction of kinesin with MTs (Hagiwara et al., 1994). To delineate whether the reduced mitochondrial movement caused by Tau 3D expression was due to increased inhibition of the motor-MT interaction by Tau 3D, we examined the binding of the kinesin motor domain fragment RK430 to MTs in the presence of Tau WT, 3A, or 3D. We used the head domain of kinesin because the tail domain also has a MT-binding domain, which competes with Tau in *in vitro* MT-binding experiments (Seeger and Rice, 2010). Histidine-tagged kinesin (kinesin-His) that was bound or not bound to MTs was detected by Coomassie staining (Fig. 6*A*) and Western blotting (Fig. 6*B*) of the MT pellets and supernatants after centrifugation. Increasing the amount of Tau WT or Tau mutants did not alter the binding of RK430 kinesin-His to MTs even though excess Tau was added such that unbound Tau appeared in the supernatant. Thus, the reduced mitochondrial movement was not caused by inhibiting the interaction between the kinesin head domain and MTs.

The phosphorylation mimic Tau 3D increases MT spacing in processes of Sf9 cells

Tau is a space-making protein between MTs (Chen et al., 1992; Frappier et al., 1994; Marx et al., 2000). We examined the effect of phosphorylation at the AT8 sites on MT spacing *in vitro*. MTs were polymerized in the presence of Tau and pelleted by centrifugation. Thin-section electron micrographs of MTs cut perpendicularly to the MT axis are shown in Figure 7*A–C*. The inter-MT distances were

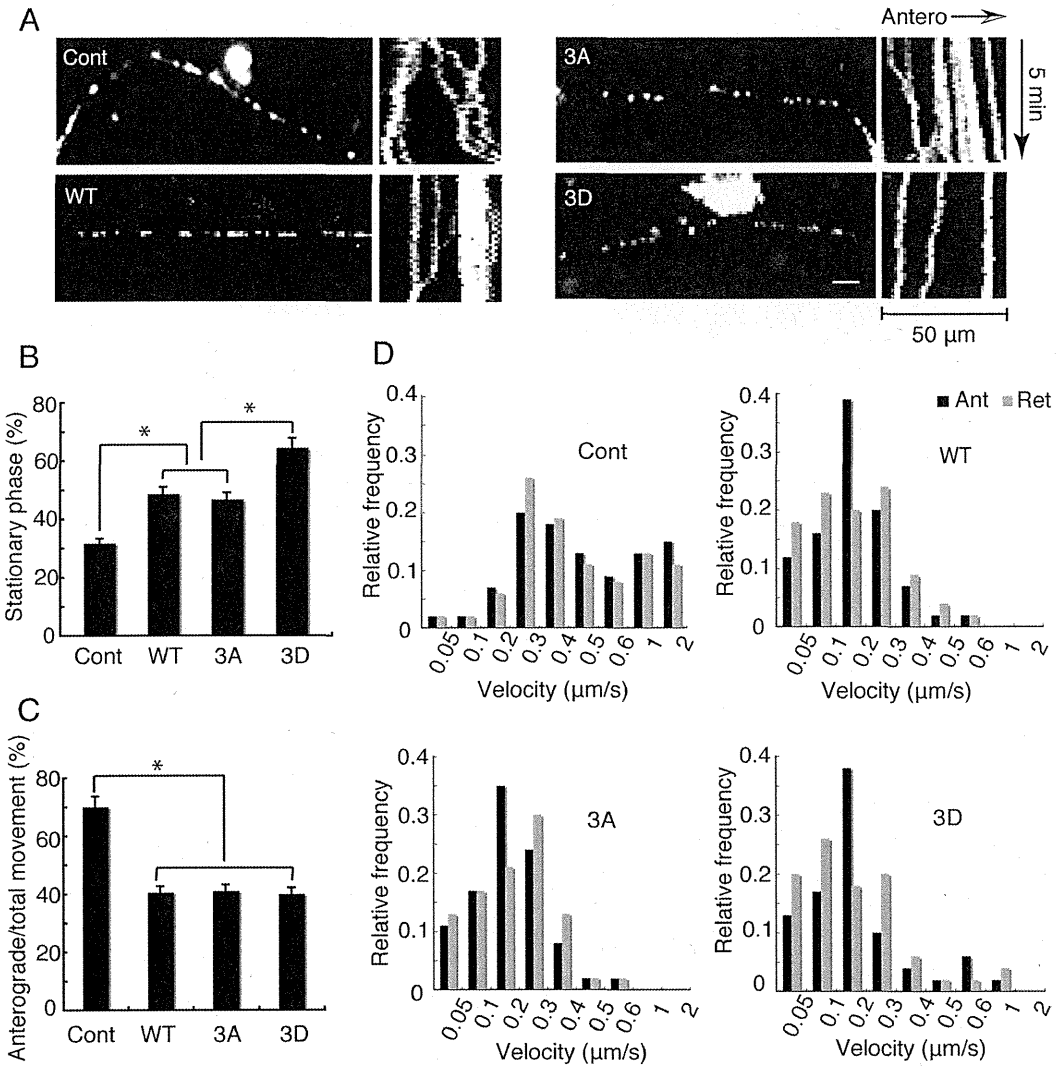

Figure 5. Reduced motile behavior of mitochondria in Tau-overexpressing neurons. ***A***, Mitochondrial distribution and movements in axons of neurons. Cultured neurons at DIV6 were transfected with Mito-GFP vector alone (Cont, Control) or cotransfected with Mito-GFP and Tau WT, Tau 3A, or Tau 3D vector. Mitochondrial distribution is shown by fluorescence of Mito-GFP (left panels). Bar, 20 μm. Right panels are kymographs of mitochondria moving in axon of neurons. Antero, Anterograde. ***B***, The percentage ratio of pausing mitochondria in axon of cultured neurons. The pausing duration was expressed as the percentage of total observation period ($n = 35$, $^*p < 0.01$, one-way ANOVA,). ***C***, The effect of Tau mutants on anterograde or retrograde movement of mitochondria. The vertical axis is the ratio of anterogradely moving duration to total moving period. The results were analyzed statistically by ANCOVA as described in Materials and Methods. The ratio was significantly different between control and Tau-overexpressing neurons ($p < 0.01$) but was not different between three Tau constructs ($p = 0.55$). ***D***, Effect of Tau mutants on the velocity of mitochondria. Relative frequencies of mitochondria moving at the indicated velocities are shown in control neurons or in neurons expressing Tau WT, Tau 3A, or Tau 3D. Black represents anterograde (Ant) movement, and gray represents retrograde (Ret) movement ($n = 35$ mitochondria per sample).

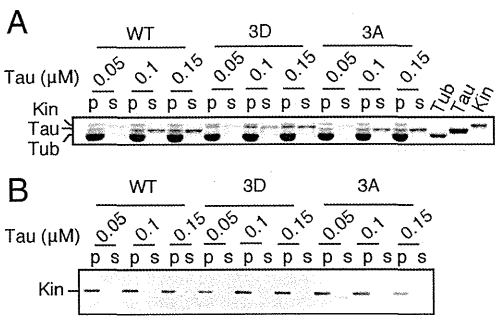

Figure 6. Tau does not inhibit the binding of kinesin to MTs. ***A***, Coomassie staining of an SDS-PAGE gel to show the binding of kinesin to MTs independent of Tau-binding. MTs polymerized in the presence of 0.05, 0.1, or 0.15 μM Tau WT, 3A, or 3D were incubated with 0.1 μM kinesin head domain-His and, after separation of MTs by centrifugation, the MT pellet (p) and supernatant (s) were subjected to SDS-PAGE. The right side three lanes are tubulin (Tub), Tau WT (Tau), and kinesin (Kin) head domain-His, respectively, for references. ***B***, An immunoblot confirming the binding of kinesin to MTs. MT pellet (p) and supernatant (s) shown in ***A*** are immunoblotted with anti-His antibody for detection of kinesin head domain-His.

measured from wall to wall of nearest-neighbor MTs. The distances were typically <10 nm in the MT pellets polymerized with Tau WT, 3A, and 3D (Fig. 7*D*), indicating that the phosphorylation-mimicking mutation at Ser199/Ser202/Thr205 did not affect the inter-MT spacing in pelleted MTs.

To determine whether this was the case in cells, we employed an Sf9 cell overexpression system that was used for Tau-induced MT bundle formation (Kanai et al., 1989; Frappier et al., 1994). We measured the distances between the nearest-neighbor MTs in the MT bundles formed in the process of Sf9 cells after infection of cells with baculovirus encoding Tau. Electron micrographs of processes in which most MTs were cut perpendicularly are shown in Figure 7, *E–G*, and the inter-MT distances are shown in Figure 7*H*. Of the 85 inter-MT distances measured, there was no significant difference between cells infected with the various Tau proteins (Fig. 7*H*). Because only a small number of processes were formed by Tau overexpression alone, however, the number of inter-MT distances we counted was not sufficient.

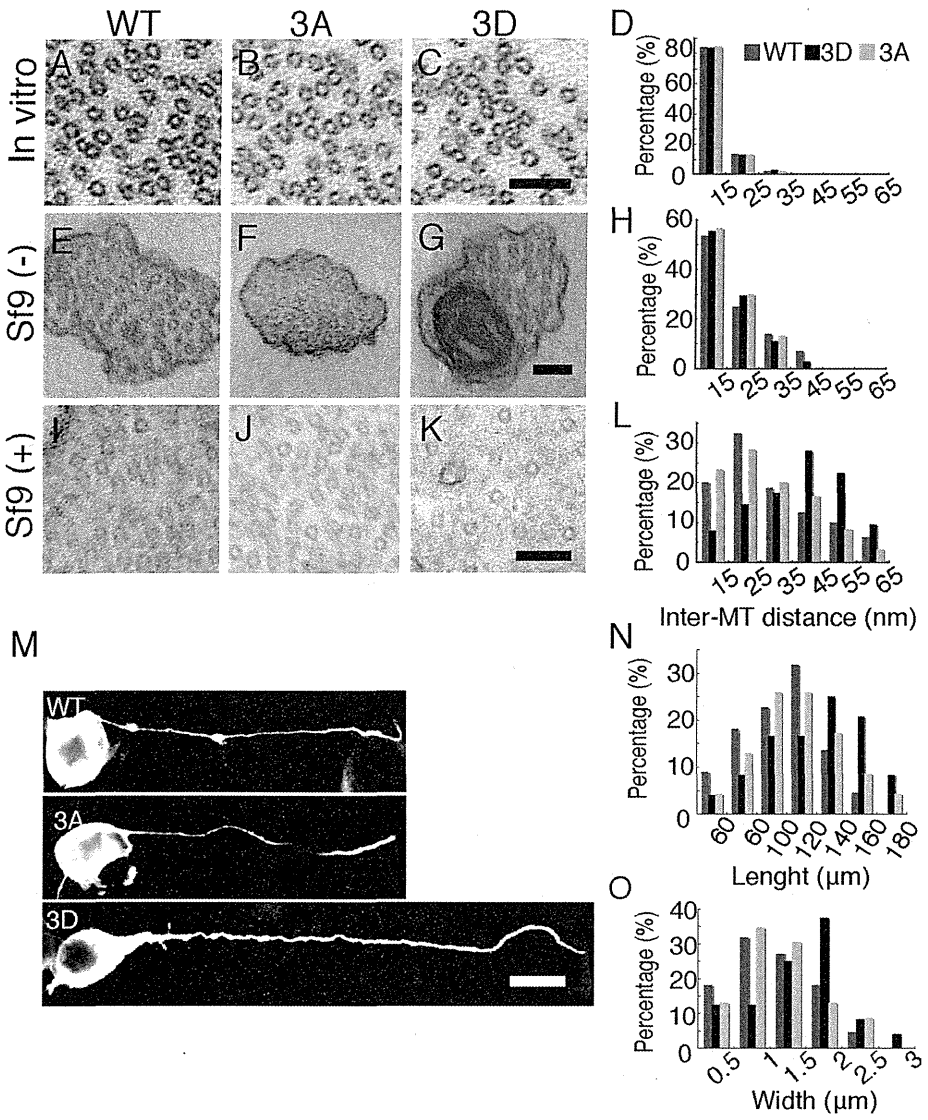

Figure 7. Inter-MT distance in MT bundles in the presence of Tau mutants. ***A–C***, Electron micrographs of cross-sections of MT pellets polymerized *in vitro* with Tau WT (***A***), 3A (***B***), or 3D (***C***). Scale bar, 100 nm. ***D***, The wall-to-wall distances between nearest-neighbor MTs were measured and expressed as the percentage of the total number of counted MTs. The mean distance was 11.7 ± 1.7 nm for Tau WT ($n = 48$), 11.8 ± 2.1 nm for Tau 3A ($n = 51$), and 11.9 ± 1.6 nm for Tau 3D ($n = 69$). ***E–G***, Electron micrographs of processes of Sf9 cells [untreated (−)] expressing Tau WT (***E***), 3A (***F***), or 3D (***G***). ***H***, Inter-MT distances were measured between nearest-neighbor MTs and expressed as the percentage of the total number of counts. The mean distance was 15.7 ± 2.2 nm for Tau WT ($n = 30$), 17.5 ± 2.7 nm for Tau 3A ($n = 27$), and 16.3 ± 2.2 nm for Tau 3D ($n = 28$). *I–K*, Electron micrographs of processes of latrunculin B-treated (+) Sf9 cells expressing Tau WT (***I***), 3A (***J***), or 3D (***K***). Sf9 cells were treated with 0.5 μg/ml latrunculin B for 72 h after infection with baculovirus expressing each Tau. ***L***, Inter-MT distances were measured and expressed as the relative ratio of the total number of counts. The mean distance was 26.8 ± 2.7 nm for Tau WT ($n = 60$), 27.2 ± 2.0 nm for Tau 3A ($n = 80$), and 37.1 ± 2.3 nm for Tau 3D ($n = 75$). ***M***, Immunostaining of Sf9 cells overexpressing Tau 3D (top), Tau 3A (middle), or WT (bottom) with anti-Tau. Scale bar, 20 μm. ***N***, ***O***, Sf9 cells overexpressing Tau 3D formed longer and wider processes compared to those expressing Tau WT or 3A. ***N***, The length distribution of Sf9 cell processes overexpressing Tau constructs. The mean length was 106.5 ± 3.7 μm for Tau WT, 97.2 ± 5.3 μm for Tau 3A, and 119.1 ± 4.3 μm for Tau 3D ($n = 20$ for each Tau construct). ***O***, The width distribution of Sf9 cell processes overexpressing Tau constructs. The mean width was 1.09 ± 0.04 μm for Tau WT, 1.04 ± 0.09 μm for Tau 3A, and 1.39 ± 0.07 μm for Tau 3D ($n = 20$ for each Tau construct).

We therefore treated Tau-overexpressing Sf9 cells with latrunculin B, which disrupts actin filaments, to increase the number of processes (Knowles et al., 1994). When the processes were stained with anti-Tau antibody, we noticed that Sf9 cells expressing Tau 3D had larger and longer processes than cells expressing Tau WT or 3A (Fig. 7*M–O*). The mean length was 106.5 ± 3.7 μm for Tau WT, 97.2 ± 5.3 μm for Tau 3A, and 119.1 ± 4.3 μm for Tau 3D (Fig. 7*N*). The mean diameter was 1.09 ± 0.04 μm for Tau WT, 1.04 ± 0.09 μm for Tau 3A, and 1.39 ± 0.07 μm for Tau 3D (Fig. 7*O*). We then observed MTs in processes by electron microscopy (Fig. 7*I–K*). The inter-MT distances were greater in Tau 3D-overexpressing cells compared to those overexpressing WT or 3A (Fig. 7*L*). Although most distances fell in the range of 15–25 nm in Tau WT- and 3A-expressing cells (mean distance = 26.8 ± 2.7 and 27.2 ± 2.0 nm, respectively), almost same as the previous results (Frappier et al., 1994), that range was 35–45 nm in Tau 3D-expressing cells (mean distance = 37.1 ± 2.3 nm) (Fig. 7*L*). Because latrunculin B reduces membrane tension by depolymerizing submembranous actin filaments, these results suggested that, under reduced tension, phosphorylation of Tau at the AT8 sites increases the space between MTs.

Tau overexpression reduces the inter-MT distances in neurites of PC12 cells

We wanted to know how expression of Tau 3A or 3D affects the inter-MT distance in axons or neuritic processes. We performed

the experiments with PC12 cells in which mitochondrial movements were affected by Tau expression as was observed in neuronal axons. Typical electron micrographs are shown in Figure 8A. More MTs were found in neurites of PC12 cells overexpressing Tau. The inter-MT distances were reduced to ~35 nm in Tau-expressing processes from ~45 nm in the control untransfected processes (Fig. 8*B*). In contrast, there was no significant difference in the inter-MT distances among Tau WT, 3A, and 3D overexpression (Fig. 8*B*). The mean distance was 33.1 ± 2.4 nm for Tau WT, 34.1 ± 2.6 nm for Tau 3A, and 34.19 ± 2.8 for 3D.

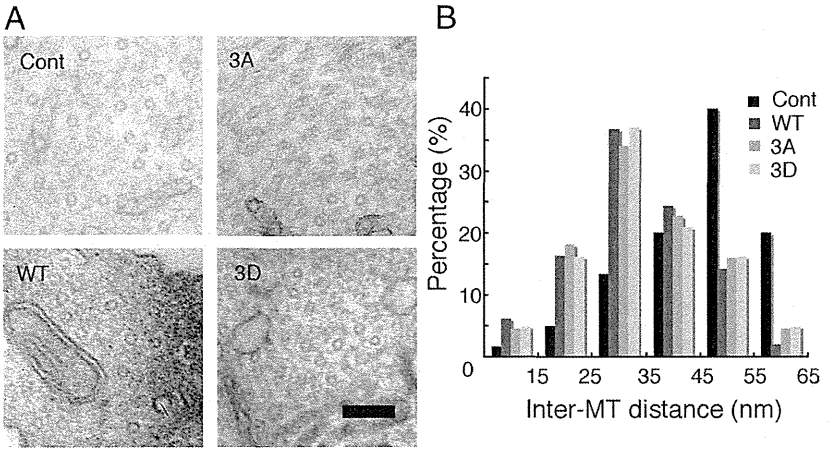

Figure 8. The distance between MTs in PC12 cell neurites overexpressing Tau constructs. ***A***, Cross-sectional electron micrographs of PC12 cell neurites, control (Cont) or overexpressing Tau WT, 3A, or 3D. Scale bar, 100 nm. ***B***, Inter-MT distances were measured between nearest-neighbor MTs and expressed as the percentage of the total number of counts. The mean distance was 45.1 ± 2.2 ($n = 54$) for control PC12 cells and 33.1 ± 2.4 nm ($n = 49$), 34.1 ± 2.6 nm ($n = 44$), and 34.19 ± 2.8 nm ($n = 62$) for PC12 cells overexpressing Tau WT, 3A, and 3D, respectively.

Discussion

Tau is a major MAP in axons and plays a role in regulating organelle transport and the dynamics of axonal MTs. Many reports have described the inhibition of mitochondrial transport by overexpressing Tau (Ebneth et al., 1998; Trinczek et al., 1999; Stamer et al., 2002; Dixit et al., 2008; Dubey et al., 2008; Stoothoff et al., 2009; Vossel et al., 2010). However, the molecular mechanism has not been determined. We studied the effect of AT8 Alzheimer phosphorylation (Ser199/Ser202/Thr205) of Tau on mitochondrial movement and found that the phosphorylation mimetic form, Tau 3D, inhibited mitochondrial transport to a greater degree than Tau WT and Tau 3A. Based on these findings together with the observation that the inter-MT distance was greater in MT bundles containing Tau 3D, we would like to propose that phosphorylation of Tau at the AT8 sites affects the transport of mitochondria along MTs by changing the inter-MT spaces.

Tau is a phosphoprotein with multiple phosphorylation sites; mass spectroscopic analysis indicates ten and five major sites in fetal and adult rat brains, respectively (Watanabe et al., 1993; Morishima-Kawashima et al., 1995; Planel et al., 2002). Major phosphorylation sites are in the Ser-Pro and Thr-Pro sequences, and most of them are in the region flanking the MT-binding domain. Phosphorylation at these sites reduces, but does not abolish, Tau binding to MTs, leading to more dynamic MTs (Wada et al., 1998; Liu et al., 2007). However, site-specific functions have not been completely investigated. Among the many Ser/Thr phosphorylation sites, Ser199, Ser202, and Thr205, which contain the recognition epitope for the AT8 monoclonal antibody, are particularly interesting. The AT8 sites are not only physiological phosphorylation sites (Kimura et al., 2007; Verwer et al., 2007) but also markers of hyperphosphorylation in Alzheimer's disease (Plattner et al., 2006). The Ser199/Ser202/Thr205 sites are present in the border between the N-terminal projection region and the MT-binding region. According to the paperclip structural model of Tau (Jeganathan et al., 2006), the site near Ser199/Ser202/Thr205 folds and the N-terminal region is situated close to the MT-binding repeats. When the Ser199/Ser202/Thr205 sites are phosphorylated the N-terminal domain swings away from the C-terminal domain, resulting in a conformation that extends from the MT wall (Jeganathan et al., 2008). The extended projection may increase the distance between MTs, although this idea has not been validated. By observing MT bundles in Sf9 cell processes treated with latrunculin B, we found that the inter-MT distance in MT bundles containing Tau 3D was longer than that in MT bundles containing Tau WT or Tau 3A.

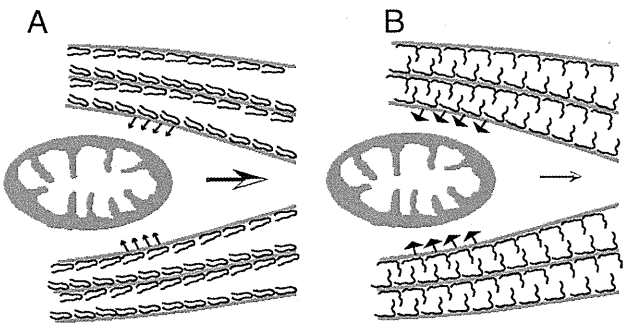

Figure 9. Schematic representation of the greater impact of Tau phosphorylation on mitochondrial transport compared to nonphosphorylated Tau. ***A***, Tau is a space-making protein attached to the MT surface. When Tau is not phosphorylated at Ser199/Ser202/Thr205, the N-terminal domain is folded. This conformation does not produce much resistance force against mitochondrial movement because MTs are in relatively close proximity. ***B***, Tau phosphorylation at Ser199/Ser202/Thr205 may extend the projection domain away from the MT surface, increasing the repulsive forces between MTs. In this conformation, mitochondria encounter greater MT resistance to the slowing or arresting of their movement.

Tau overexpression inhibits mitochondrial movement in various cell types (Ebneth et al., 1998; Trinczek et al., 1999; Stamer et al., 2002; Dixit et al., 2008; Stoothoff et al., 2009; Vossel et al., 2010). We also observed an inhibition of mitochondrial movement in PC12 cells and cortical neurons. Tau WT overexpression increased the pausing frequency from 31.6 to 48.5% in neurons, which is almost identical to previous results (Stamer et al., 2002). Overexpression of either Tau WT, 3A, or 3D reduced anterograde movement of mitochondria in PC12 cells and cortical neurons, as reported (Mandelkow et al., 2004; Hollenbeck and Saxton, 2005; Dixit et al., 2008). Furthermore, the velocity was reduced similarly in both directions by Tau overexpression regardless of its phosphorylation state, although the inhibition profile differed slightly among the three Tau constructs. Thus, Tau clearly inhibits mitochondrial transport independent of its phosphorylation state. Several models have been proposed for Tau-mediated inhibition of mitochondrial transport: overstabilization of MTs (Shemesh et al., 2008), competition between motor proteins for interaction with the MT surface (Hagiwara et al., 1994), and in-

hibition of motor protein access to MTs (Seeger and Rice, 2010). Another mechanism proposed recently involves the distance between MTs (Thies and Mandelkow, 2007). When Tau is overexpressed in cortical neurons, tubulin synthesis is upregulated and MTs become more numerous and densely packed, resulting in inhibition of mitochondrial movement. This observation was in dendrites, but similar Tau overexpression-induced increases in MTs were reported in axons (Sudo and Baas, 2010). We observed here that Tau overexpression increased the number of MTs and reduced the inter-MT spaces in neurites of PC12 cells. Our observation is consistent with the last model described above. Considering that mitochondria would be transported within MT bundles in cultured neurons (Yu and Baas, 1994; Rochlin et al., 1996), limited spacing between MTs may block mitochondrial movement in neuritic processes such as axon and dendrites.

We found that Tau 3D more potently inhibited mitochondrial transport than Tau WT or Tau 3A. Phosphorylation of Tau at the AT8 sites has an additional inhibitory action on mitochondrial movement over the Tau molecule itself. We hypothesize that the inhibition caused by Ser199/Ser202/Thr205 phosphorylation relates to the distance between MTs. The inter-MT distance was the same (15–25 nm) in MT bundles formed by Tau WT, 3A, and 3D in Sf9 cell processes, but it was expanded to 35–45 nm in processes expressing Tau 3D when actin filaments were disrupted by latrunculin B. Actin filaments are abundant in submembranous regions, providing tension to plasma membranes. As reported (Knowles et al., 1994), disassembly of actin filaments increases the number of processes induced by Tau overexpression. Phosphorylation-dependent expansion of the space between MTs was observed only with reduced membrane tension. The force produced by outward extension of the projection domain may not be strong enough to push surrounding MTs against the membrane, which may explain why phosphorylation-induced expansion of the inter-MT distance has not been reported.

Axons are long processes that extend ~1 m or more. To maintain axonal structures to over 80 years in humans, the axoplasm is filled with cytoskeletal components, and the outer surface is surrounded by thick myelin. These features may indicate that the axoplasmic MT milieu is under the strong tension (Yu and Baas, 1994; Rochlin et al., 1996). Phosphorylation of Tau at the AT8 sites tends to increase the inter-MT distance, but under strong tension the inter-MT distance cannot expand (Fig. 8), and instead the repulsive forces between MTs increase (Fig. 9). Increased repulsive forces between MTs would generate a stronger reactive resistance against mitochondria moving inside MT bundles. The AT8 sites are physiological sites for phosphorylation, but they are not always phosphorylated (Kimura et al., 2007; Verwer et al., 2007). The AT8 sites may be interconverted between phosphorylated and dephosphorylated states depending on the cell's need for mitochondrial movement. Dephosphorylation ahead of moving mitochondria would reduce the repulsive force between adjacent MTs for mitochondrial passage, and rephosphorylation of Tau behind mitochondria may facilitate the directional movement of mitochondria (Shahpasand et al., 2008). Of course, phosphorylation-dependent tunnel opening and closing for mitochondrial movement is expected to be coordinated with activities of motor proteins, protein kinases, and protein phosphatases. This is our working hypothesis, which we will explore further in the future.

We used PC12 cells and cultured cortical neurons in this study in which MTs are major cytoskeletal components. In matured or aged neurons, however, Tau may not be the only space-making protein that affects mitochondrial movement in a phosphorylation-dependent manner. The C-terminal tail domains of neurofilament M and H subunits extrude outward from core filaments, as does the projection domain of Tau, to make spaces between neurofilaments (NFs) (Hisanaga and Hirokawa, 1989). NFs are highly phosphorylated in aged axons and AD neurodegenerative disease (Uchida et al., 2004; Rudrabhatla et al., 2010). Hyperphosphorylation of the tail domains would increase the inter-NF distances to expand the NF domain in axons (Kumar et al., 2002; Kanungo et al., 2011), giving higher pressure to the MT domain. This would suppress mitochondrial transport along MTs by restricting radial displacement of MTs. Thus, mitochondrial movements in aged and neurodegenerative axons would be affected in a more complicated manner.

AT8 reactivity has been frequently used as an indicator of hyperphosphorylation of Tau in AD brains or other tauopathies (Stoothoff and Johnson, 2005; Hanger et al., 2009). Impairment of mitochondrial traffic is also a feature of tauopathies (Stokin et al., 2005; Lippens et al., 2007). An unanswered issue is whether abnormal Tau phosphorylation is caused by impaired organelle trafficking or if blocked transport is a consequence of abnormal phosphorylation. Using the phosphorylation mimic Tau 3D, we showed that Tau phosphorylation within the AT8 sites inhibited mitochondrial transport more effectively than in experiments carried out with Tau WT and Tau 3A. Because Tau 3A and 3D have similar phosphorylation profiles at other sites, the observed effect is likely caused by phosphorylation at Ser199/Ser202/Thr205. Thus, our results suggest that the increased phosphorylation of the AT8 sites in brains of Alzheimer's patients decreases mitochondrial transport in axons, leading to axonal degeneration. Our current study not only leads us to focus on the AT8 sites with regard to Alzheimer's therapeutics but also indicates the effectiveness of a similar strategy addressing other abnormal phosphorylation sites on mitochondrial movement.

References

Bereiter-Hahn J, Jendrach M (2010) Mitochondrial dynamics. Int Rev Cell Mol Biol 284:1–65.

Bershadsky AD, Gelfand VI, Svitkina TM, Tint IS (1978) Microtubules in mouse embryo fibroblasts extracted with Triton X-100. Cell Biol Int Rep 2:425–432.

Chen J, Kanai Y, Cowan NJ, Hirokawa N (1992) Projection domains of MAP2 and tau determine spacings between microtubules in dendrites and axons. Nature 360:674–677.

Darios F, Muriel MP, Khondiker ME, Brice A, Ruberg M (2005) Neurotoxic calcium transfer from endoplasmic reticulum to mitochondria is regulated by cyclin-dependent kinase 5-dependent phosphorylation of tau. J Neurosci 25:4159–4168.

Dixit R, Ross JL, Goldman YE, Holzbaur EL (2008) Differential regulation of dynein and kinesin motor proteins by tau. Science 319:1086–1089.

Dubey M, Chaudhury P, Kabiru H, Shea TB (2008) Tau inhibits anterograde axonal transport and perturbs stability in growing axonal neurites in part by displacing kinesin cargo: neurofilaments attenuate tau-mediated neurite instability. Cell Motil Cytoskeleton 65:89–99.

Ebneth A, Godemann R, Stamer K, Illenberger S, Trinczek B, Mandelkow E (1998) Overexpression of tau protein inhibits kinesin-dependent trafficking of vesicles, mitochondria and endoplasmic reticulum: implications for Alzheimer's disease. J Cell Biol 143:777–794.

Endo R, Saito T, Asada A, Kawahara H, Ohshima T, Hisanaga S (2009) Commitment of 1-methyl-4-phenylpyrinidinium ion-induced neuronal cell death by proteasome-mediated degradation of p35 cyclin-dependent kinase 5 activator. J Biol Chem 284:26029–26039.

Frappier TF, Georgieff IS, Brown K, Shelanski ML (1994) Tau Regulation of microtubule-microtubule spacing and bundling. J Neurochem 63:2288–2294.

Furuta K, Edamatsu M, Maeda Y, Toyoshima YY (2008) Diffusion and di-